

DTIC FILE COPY

(4)

Dr. Michael D. Seltzer
A.S.E.E./ONT Postdoctoral Fellow
October 1986 - October 1988
Chemistry Division, Research Department
Instrumental Chemical Analysis Branch
NAVAL WEAPONS CENTER
China Lake, California 93555

Final Technical Report

AD-A200 544

DTIC
ELECTE
OCT 12 1988
S D
CD
D

DISTRIBUTION STATEMENT A
Approved for public release
Distribution Unlimited

88 1011 268

Dr. Michael D. Seltzer
 A.S.E.E./ONT Postdoctoral Fellow
 October 1986 - October 1988
 Chemistry Division, Research Department
 Instrumental Chemical Analysis Branch
 NAVAL WEAPONS CENTER
 China Lake, California 93555

Final Technical Report

Contents:

1. An Active Nitrogen Plasma Atom Reservoir for Laser-Induced Ionization Spectrometry, M.D. Seltzer and R.B. Green, Spectroscopy Letters **20(8)** (1987) 601
2. Laser-Induced Ionization Spectrometry: Alternate Atom Reservoirs R.B. Green and M.D. Seltzer, Proceedings, Lasers '87, Dec. 7-11, 1987
3. Optogalvanic Spectroscopy in a Microwave-Induced Active Nitrogen Plasma, M.D. Seltzer, E.H. Piepmeier, and R.B. Green Applied Spectroscopy, **42** (1988) 1039
4. Direct Laser Ionization in Analytically-Useful Flames M.D. Seltzer and R.B. Green, Applied Spectroscopy, Accepted 1988
5. Laser Power Dependency of Resonance Ionization in Flames M.D. Seltzer and R.B. Green, Applied Spectroscopy, Submitted 1988
6. Electrical Characteristics of Microwave-Induced Plasmas for Laser-Induced Ionization Spectrometry, M.D. Seltzer and R.B. Green, Spectroscopy Letters, Submitted, 1988



Accession For	
NTIS GRA&I	<input checked="" type="checkbox"/>
DTIC TAB	<input type="checkbox"/>
Unannounced	<input type="checkbox"/>
Justification	
By	<i>lts on file</i>
Distribution	
Availability Codes	
Dist	Avail and/or Special
A-1	

AN ACTIVE NITROGEN PLASMA ATOM RESERVOIR
FOR LASER-INDUCED IONIZATION SPECTROMETRY

Key Words: Active Nitrogen, Laser-enhanced Ionization,
Dual Laser Ionization

Michael D. Seltzer and Robert B. Green

Research Department, Chemistry Division (Code 3851)
Naval Weapons Center, China Lake, CA 93555

ABSTRACT

A microwave-induced, atmospheric pressure active nitrogen plasma has been investigated as an atom reservoir for laser-induced ionization spectrometry. Discrete analyte samples were introduced into the active nitrogen plasma by a microarc atomizer. Both laser-enhanced ionization (LEI) and dual laser ionization (DLI) were carried out in the plasma plume that extended from the Beenakker cavity.

AN ACTIVE NITROGEN PLASMA ATOM RESERVOIR
FOR LASER-INDUCED IONIZATION SPECTROMETRY

Key Words: Active Nitrogen, Laser-enhanced Ionization,
Dual Laser Ionization

Michael D. Seltzer and Robert B. Green

Research Department, Chemistry Division (Code 3851)
Naval Weapons Center, China Lake, CA 93555

ABSTRACT

A microwave-induced, atmospheric pressure active nitrogen plasma has been investigated as an atom reservoir for laser-induced ionization spectrometry. Discrete analyte samples were introduced into the active nitrogen plasma by a microarc atomizer. Both laser-enhanced ionization (LEI) and dual laser ionization (DLI) were carried out in the plasma plume that extended from the Beenakker cavity.

INTRODUCTION

Because of its interesting energetic properties, the active nitrogen plasma has been investigated as an alternative to the

analytical flame as an atom reservoir for laser-induced ionization spectrometry. The laser-induced ionization techniques examined in this study were laser-enhanced ionization (LEI) and dual laser ionization (DLI). Ionization from a laser-excited state proceeds by collisional processes in the former case and absorption of photons in the latter.

LEI spectrometry is among the most sensitive methods available for trace metal analysis. Detection limits reported for LEI¹⁻⁴ are comparable to those reported for laser-excited atomic fluorescence spectrometry [LEAFS].^{5,6} LEI has several advantages over conventional spectroscopic methods, including nonoptical detection and an abundance of usable transitions within a relatively narrow spectral range which makes possible the excitation of several elements by using a single laser dye.⁴

LEI and DLI⁷ may be viewed as complementary techniques and are similar in their implementation and methodology. LEI occurs whenever a laser is tuned to a resonance transition of an atom in a flame. Whether or not an additional photoionizing laser will supplement the LEI signal depends on how closely its wavelength matches the energy defect between the laser-excited level and the ionization potential of the analyte atom.⁸ The atom reservoir is also an important consideration. Photoionization makes a greater contribution to the total ionization signal (i.e., current) in atom reservoirs where the rate of collisional ionization is relatively low, such as a hydrogen-oxygen-argon flame.^{7,8} Photoionization of a laser-excited atom usually requires the addition of a second laser, but there are cases where a single laser may be adequate, or a third laser may be required.

Most of the laser-induced ionization studies, to date, have employed analytical flames as atom reservoirs. Flames are commonly used to desolvate and atomize samples for spectrometry. In

addition, they provide effective collisional cells for LEI. However, spectroscopic techniques that employ flames can be limited by interferences associated with flame atomization and ionization. This is most evident in laser-induced ionization techniques where group IA and IIA elements interfere with signal (i.e., ion) collection. These elements are easily ionized in the flame, resulting in the formation of a positive ion sheath which shields the cathode and, consequently, suppresses the analyte ionization signal. This problem has been effectively addressed for LEI in air/acetylene flames by the use of the immersed cathode which permits laser enhancement within the collecting field.⁹ Use of the immersed cathode has allowed complete LEI signal recovery from samples containing high sodium concentrations.

The most significant LEI improvements have resulted from changes in electrode design,⁹ access to UV wavelengths through the use of advanced laser technology,¹⁰ and sample pretreatment for removal of interferences.¹¹ Only recently have alternative atom reservoirs for LEI received attention. Turk and Watters¹² reported the use of an argon inductively coupled plasma for LEI spectrometry. The authors attributed a lack of sensitivity to a low atom population in the plasma tail flame where the LEI measurements were carried out.

More recently, Magnusson et al.,² and Axner and Rubensztein-Dunlop³ have reported LEI detection of trace elements in a graphite furnace. Both one and two-step excitation schemes were reported. The two-step excitation scheme allowed background correction.³ The authors suggested that a change in furnace purge gas from argon to nitrogen, or a mixture of argon and methane might create a better collisional environment in the furnace. This could lead to further enhancements in ionization and, thus, higher sensitivity.

Niemczyk and Na¹³ have reviewed the fundamentals and applications of the microwave-induced active nitrogen plasma which has been demonstrated to be an efficient source for atomic emission spectrometry. Microwave-induced plasmas (MIPs) using a variety of gases and gas mixtures, have been well characterized in the literature.^{14,15} In an active nitrogen plasma, non-thermal energy transfer of up to several electron volts is possible through very efficient collisions of analyte atoms with plasma species.¹³ This is in contrast to the air/acetylene flame in which the nitrogen molecule with a Boltzmann energy of around 0.2 eV is the major collisional partner in the LEI process.¹² Hood and Niemczyk¹⁶ have recently reported excitation temperatures, measured in a low-pressure active nitrogen plasma, that are higher than in most flames. Active nitrogen is relatively easy to generate in a microwave discharge and has the potential for excitation and ionization of a large number of elements.¹⁷ Thus, the active nitrogen plasma should present a comparable, if not superior, collisional environment for LEI.

Most of the published research involving the use of active nitrogen for atomic emission was carried out at pressures below atmospheric using low microwave power (<100 W). Low power microwave-induced plasmas are very efficient excitation sources, but lack the thermal energy required to vaporize samples. In the past, conventional sample introduction into MIPs presented many difficulties including the plasma's intolerance for sample solvent.¹⁴ Successful liquid aerosol sample introduction into a low power MIP has recently been reported however.¹⁸

In the present study, a microarc atomizer was used to introduce discrete samples into a microwave-induced, atmospheric pressure active nitrogen plasma. Deutsch and Hieftje¹⁹ used a microarc atomizer to introduce samples into a microwave-induced nitrogen plasma for atomic emission studies. The microarc

atomizer separates sample desolvation and atomization steps. It employs both sputtering and thermal desorption to efficiently atomize small samples.²⁰ The microarc atomizer has more recently been explored as an atomic emission source²¹ and as an atom reservoir for LEI and DLI.²²

The preliminary results presented here demonstrate the feasibility of using an active nitrogen plasma atom reservoir for both LEI and DLI spectrometry. LEI has also been observed in an MIP by Lysakowski.²³ In the present work, a comparison of LEI and DLI signals for indium indicates that DLI photoionization enhancement⁸ of the LEI signal is small. These results suggest that the rate of collisional ionization in the active nitrogen plasma may be comparable to typical analytical flames.

EXPERIMENTAL SECTION

A schematic diagram of the instrumentation used in this study is given in Figure 1. A linear flashlamp-pumped dye laser (CMX-4, Chromatix), with a 0.8 μ s pulse length and frequency doubling capability, was used as the excitation source for all experiments. The laser was operated with rhodamine 590 at a repetition rate of 30 Hz. A UV-transmitting, visible absorbing filter was used to block the laser fundamental output during the LEI experiments. The laser wavelength was optimized prior to each experiment by observing the optogalvanic effect in a hollow cathode lamp. A standard LEI detection system was used, including a preamplifier²⁴ and a boxcar signal averager, for signal processing. A strip chart recorder provided the signal readout.

Active Nitrogen Plasma

An active nitrogen plasma was generated using a laboratory-constructed Beenakker type microwave cavity.²⁵ The microwave power oscillator (Micro-Now, Skokie, IL) was used to deliver powers between 50 and 150 W. The microwave cavity was carefully designed so that reflected power was always less than 10% of the forward power value, and in some cases, was too small to measure accurately. The active nitrogen plasma plume was generated at atmospheric pressure by exciting a mixture of argon (1.2 L/min) and nitrogen (10-50 mL/min). The nitrogen was obtained from liquid nitrogen boil-off. The atmospheric pressure plasma was chosen over a low-pressure plasma (<10 Torr) to facilitate sample introduction and eliminate the need for a vacuum system. An 8-mm I.D. x 150-mm long quartz tube was used to direct the gas mixture through the microwave cavity. The tube extended about 100 mm beyond the cover plate of the microwave cavity. The active nitrogen plasma plume extended about 50 to 60 mm beyond the end of the quartz tube. The plasma plume exhibited the active nitrogen afterglow; the characteristic yellow emission was monitored using a diode-array spectrometer (Tracor-Northern, Middleton, WI). The most stable plasma conditions were obtained with applied microwave powers in the range of 60 to 70 W and nitrogen flow rates between 30 and 40 mL/min.

Signal Collection

The laser beam was directed along the longitudinal axis of the plasma plume. Ion collection electrodes (12 x 60 mm) were positioned on either side of the plasma plume and were separated by a distance of 10 to 12 mm. The electrodes were operated at a potential of -1500 V. At potentials higher than this, arcing through the plasma plume occurred. The plasma plume, ion collection electrodes, and preamplifier were shielded by a copper screen

and plexiglass enclosure to minimize pickup of RF interference from the laser, eliminate drafts, and to facilitate the exhausting of ozone.

Microarc Atomizer

A laboratory-constructed microarc atomizer was positioned at the rear of the Beenakker cavity in direct line with the gas flow to the plasma. This arrangement was found to facilitate sample transport to the plasma. The gas flow through the microarc and Beenakker cavity was higher than the flow rate normally used in a microarc atomizer but close to the minimum flow rate required to sustain the microwave plasma. Therefore, the gas flow rate used was a compromise between a stable plasma and optimum operation of the microarc. A tungsten rod was used as an anode and a nichrome wire loop was used as the cathode. The sample was desolvated by resistive heating of the wire. When a 1- μ L sample droplet was placed on the cathode, a visible change in the active nitrogen emission spectrum was observed. The presence of water in the plasma resulted in a momentary quenching of the nitrogen afterglow. The completion of sample desolvation was indicated by the reappearance of the yellow nitrogen afterglow in the plasma plume. The microarc power supply is described in Refs. 21 and 22.

LEI Measurements

Indium was chosen as a test element for the initial experiments because of the proximity of one of its resonance lines to a peak in the frequency-doubled tuning curve of rhodamine 590. Excitation at the indium resonance line at 303.9 nm resulted in promotion to a level that was within 1.70 eV of the 5.78 eV ionization potential of indium. Energetically, these are favorable conditions for a good LEI yield in a collisional environment. LEI

measurements for 10-ng samples of indium were made while adjusting the plasma parameters of applied microwave power and nitrogen gas flow. These parameters directly affected the concentration of plasma species and, hence, the collisional efficacy of the plasma.

An experiment was carried out to determine whether the resonant transition at 303.9 nm was optically saturated. The laser beam was attenuated with calibrated neutral density filters and the corresponding LEI signals for replicate 10 ng samples of indium were recorded. A plot of LEI signal vs. laser power revealed a non-linear dependence of LEI signal at the higher laser powers. Optical saturation of this transition helped minimize the effect of pulse-to-pulse amplitude differences in laser output on the outcome of the indium LEI experiments.

DLI Measurements

DLI studies usually require the addition of a second laser to photoionize laser-excited analyte atoms. In this case, a DLI excitation scheme for indium was conveniently arranged using a single dye laser with both frequency-doubled and fundamental output beams.²² The fundamental laser wavelength of 607.8 nm was frequency doubled to produce the second harmonic at 303.9 nm. The 303.9 nm beam was used, as in the LEI experiments, for the excitation step. The 607.8 nm fundamental output was used for the photoionization step. The addition of the 2.04 eV ionizing photon resulted in a 0.34 eV energy overshoot beyond the ionization potential of indium. This overshoot was relatively small and, therefore, near optimal for observing a DLI enhancement over LEI.⁸

In DLI studies, the degree of overlap of the excitation and ionization laser beams in the atom reservoir is critical.⁸ The tunable dye laser used in the present study produced a second

harmonic beam that was displaced vertically above the fundamental output beam. The cross-sectional overlap between these beams was about 30%, creating a non-optimum condition for DLI enhancement. To circumvent this problem, the laser output beam was expanded and a 2-mm iris was positioned in the region where the fundamental and second harmonic overlapped. This approach allowed the plasma plume to be irradiated by a composite beam with nearly 100% overlap between the fundamental and second harmonic. The resonance transition of indium was still optically saturated despite losses in laser intensity due to expansion and spatial filtering of the beam. Comparative DLI/LEI experiments were run under the same conditions of illumination. An applied microwave power of 60 W and a nitrogen flow rate of 30 mL/min were used for the DLI measurements. These conditions provided less than optimum LEI yields (see Figs. 2, 3) but promoted the most stable plasma.

RESULTS AND DISCUSSION

Laser-enhanced ionization signals were detected for indium excited under optical saturation conditions. With the excitation step saturated, the amplitude of the ionization signal was influenced primarily by the efficacy of collisions of the excited-state analyte atoms with plasma species. The concentration of active nitrogen in the plasma was controlled by varying the nitrogen flow rate or the microwave power. The active nitrogen concentration in the plasma plume could be increased by increasing either of these two variables. The nitrogen flow rate was the predominant influence as indicated by the emission intensity of the nitrogen afterglow which was monitored with the diode-array spectrometer. Figure 2 illustrates the effect of the nitrogen flow rate on the LEI signal. The nitrogen flow rate was varied between 7 mL/min and 75 mL/min and LEI measurements were made for 10 ng aqueous samples of indium. The applied microwave

power was fixed at 60 W. The nitrogen flow rate was small in comparison with the argon flow rate, which was maintained at 1.2 L/min in order to keep the rate of sample transport through the system constant. The LEI signals were maximum at a flow rate of 7 mL/min and decreased by a factor of four as the flow rate was increased to 75 mL/min. At nitrogen flow rates lower than 7 mL/min, the plasma became unstable and began to pulsate. When the nitrogen flow was reduced to zero, the remaining argon plasma retreated back into the Beenakker cavity and LEI signals were too small to detect at the same gain setting of the boxcar. The observed decrease in LEI signal size with increasing active nitrogen concentration may have been the result of depletion in the population of ground state analyte atoms due to effective excitation and ionization of the analyte by the plasma itself.¹⁷ The reduced sensitivity for atomic fluorescence as compared to atomic emission measurements made in active nitrogen plasmas,²⁶ provides further evidence for the depletion of ground state analyte atom populations.

Figure 3 illustrates the effect of applied microwave power on the LEI signal. The microwave power was varied between 50 and 150 W and LEI measurements were made for 10-ng samples of indium. The argon and nitrogen flow rates were fixed at 1.2 L/min and 12 mL/min, respectively. Measurements were not attempted below 50 W applied power because the plasma became unstable below this power level. The LEI signal was maximum at 50 W and decreased gradually with increasing microwave power and the subsequent increase in active nitrogen concentration.

DLI Enhancement of the LEI Signal

A comparative study of DLI and LEI was carried out in the active nitrogen plasma. In both cases, indium was excited at 303.9 nm. Measurements for replicate 10 ng samples of indium were

made with and without the addition of a photoionizing beam. The addition of the photoionizing laser beam resulted in DLI signal enhancements of up to a factor of two relative to LEI measurements made under the same conditions. Since saturation of the excitation step at 303.9 nm was maintained throughout all experiments, it was assumed that laser intensity losses due to reflection off the UV transmitting-visible absorbing filter, did not contribute significantly to the difference between the LEI and DLI signal amplitudes.

A DLI detection limit based on a signal-to-noise ratio of three was estimated for indium. For quantitation purposes, the chart-recorded peak heights of the transient ionization signals were measured. The noise was taken as one-fifth the peak-to-peak noise on the baseline. A detection limit of 20 pg was estimated by extrapolation from signal-to-noise ratios of measurements made with 1-ng samples of indium. The reproducibility at this level was approximately 15% relative standard deviation. Figure 4 shows signals recorded for consecutive 1 ng indium samples. The best DLI detection limits for indium were comparable to the best obtained for LEI (using full illumination). The DLI enhancement factor offset the loss of LEI signal that was a result of reduced beam volume due to spatial filtering in the DLI/LEI comparison experiment.

Background Ionization and Limiting Noise

Measurements made in the active nitrogen plasma with the microarc atomizer turned off and no analyte present indicated the presence of low level laser-induced background ionization. Signals were observed with laser excitation both on and off the 303.9-nm line. The signals disappeared when the laser beam was blocked, leaving a baseline signal that resulted primarily from pickup of RF interference from the laser. The combination of

laser-induced plasma ionization and pickup of RF interference may present a fundamental limit on the sensitivity of this technique. An optimization of the plasma, in addition to improvements in electrical shielding and grounding, may help reduce the magnitude of these background signals and, hence, their contribution to the total noise.

CONCLUSION

The preceding results demonstrate the feasibility of using an active nitrogen plasma atom reservoir for laser-induced ionization spectrometry. Picogram level sensitivity for discrete samples of indium was obtained by both LEI and DLI techniques.

DLI enhancements of up to 1000 have been obtained for some elements by using excitation schemes with relatively small energy overshoots.⁸ The DLI enhancement observed for indium in the present study was approximately the same as reported for indium in Ref. 8, but the energy overshoot was less than half as large. Thus, a larger DLI enhancement would have been expected in the present case, providing the atom reservoirs had similar collisional properties. Although several experimental differences prevent a direct comparison between the previous results and the present work, the absence of a larger DLI enhancement for indium in the present work suggests that a higher rate of collisional ionization exists in the active nitrogen plasma relative to the hydrogen-oxygen-argon flame used in Ref. 8. The collisional properties of the active nitrogen plasma may more closely approach the air/acetylene flame.

Low ground state analyte atom populations in the active nitrogen plasma, relative to analytical flames, implies that analyte atom excited states are more highly populated in the

plasma. This is exemplified by the high sensitivity obtained for atomic emission in the active nitrogen plasma.¹³ This being the case, non-resonant LEI excitation of analyte atoms in the active nitrogen plasma should demonstrate improved sensitivity over similar excitation schemes in flames.

The microarc atomizer is currently being optimized to improve the reproducibility of atomization and, hence, the precision. Synchronization of the laser firing to the transit of the analyte "plug" through the region of the plasma sampled by the LEI electrodes would improve both precision and sensitivity.

Experiments are being planned to investigate LEI and DLI for a series of other elements to further characterize the role of the active nitrogen plasma. Initial investigations of the effect of easily-ionized elements on the analyte ionization signal indicate that the electrical interferences may be similar to those in flames.¹ High voltage interferent removal schemes²⁷ may be more effective in active nitrogen plasmas than flames. The former should more efficiently ionize IA and IIA elements, leading to a more quantitative removal.

ACKNOWLEDGMENTS

The authors gratefully acknowledge the assistance of Wayne A. Weimer (Naval Weapons Center) with the microarc atomizer. Michael D. Seltzer was supported by an Office of Naval Technology post-doctoral fellowship which is administered by the American Society for Engineering Education.

REFERENCES

1. J.C. Travis, G.C. Turk, and R.B. Green. *Anal. Chem.*, **54** (1982) 1006A.
2. I. Magnusson, O. Axner, I. Lindgren, and H. Rubensztein-Dunlop. *Appl. Spectrosc.*, **40** (1986) 968.
3. O. Axner and H. Rubensztein-Dunlop. *Laser Applications to Chemical Analysis, Topical Meeting, Incline Village, NV, January 26-29, 1987.*
4. O. Axner, I. Magnusson, J. Petersson, and S. Sjostrom. *Appl. Spectrosc.*, **41** (1987) 19.
5. S.J. Weeks and J.D. Winefordner. *Anal. Chem.*, **50** (1978) 360.
6. M.A. Bolshov, A.V. Zybin, and I.I. Smirenkinu. *Spectrochim. Acta*, **36B** (1981) 1143.
7. C.A. van Dijk, F.M. Curran, K.C. Lin, and S.R. Crouch. *Anal. Chem.*, **53** (1981) 1275.
8. F.M. Curran, K.C. Lin, G.E. Leroi, P.M. Hunt and S.R. Crouch. *Anal. Chem.*, **55** (1983) 2382.
9. G.C. Turk. *Anal. Chem.*, **53** (1981) 1187.
10. G.J. Havrilla and K.J. Choi. *Anal. Chem.*, **58** (1986) 3095.
11. G.J. Havrilla and C.C. Carter. *Laser Applications to Chemical Analysis, Topical Meeting, Incline Village, NV, January 26-29, 1987.*
12. G.C. Turk and R.L. Watters. *Anal. Chem.*, **51** (1985) 1979.
13. T.M. Niemczyk and H.C. Na. *Appl. Spectrosc. Rev.*, **19(3)** (1983) 363.
14. A.T. Zander and G.M. Hieftje. *Appl. Spectrosc.*, **35** (1981) 357.
15. K.C. Ng and M.J. Brechman. *Spectroscopy*, Vol.2 No.1 (1987) 23.
16. W.H. Hood and T.M. Niemczyk. *Appl. Spectrosc.*, **41** (1987) 674.
17. A.N. Wright and C.A. Winkler. *Active Nitrogen*, New York: Academic, 1968.

18. K.C. Ng and W.-L. Shen. *Anal. Chem.*, **58** (1986) 2084.
19. R.D. Deutsch and G.M. Hieftje. *Anal. Chem.*, **56** (1984) 1923.
20. J.P. Keilsohn, R.D. Deutsch and G.M. Hieftje. *Appl. Spectrosc.*, **37** (1983) 101.
21. R.B. Green and R.R. Williams. *Anal. Chim. Acta*, **187** (1986) 301.
22. M.E. Churchwell, T. Beeler, J.D. Messman, and R.B. Green. *Spectrosc. Lett.*, **18(9)**, (1985) 679.
23. R. Lysakowski, Virginia Polytechnic Institute & State University, personal communication.
24. G.J. Havrilla and R.B. Green. *Chem. Biomed. and Environ. Instr.*, **11(4)**, (1981) 273.
25. C.I.M. Beenakker. *Spectrochim. Acta*, **31B** (1976) 485.
26. R.G. Michel, University of Connecticut, personal communication.
27. T.O. Trask and R.B. Green. *Spectrochim. Acta*, **38B** (1983) 503.

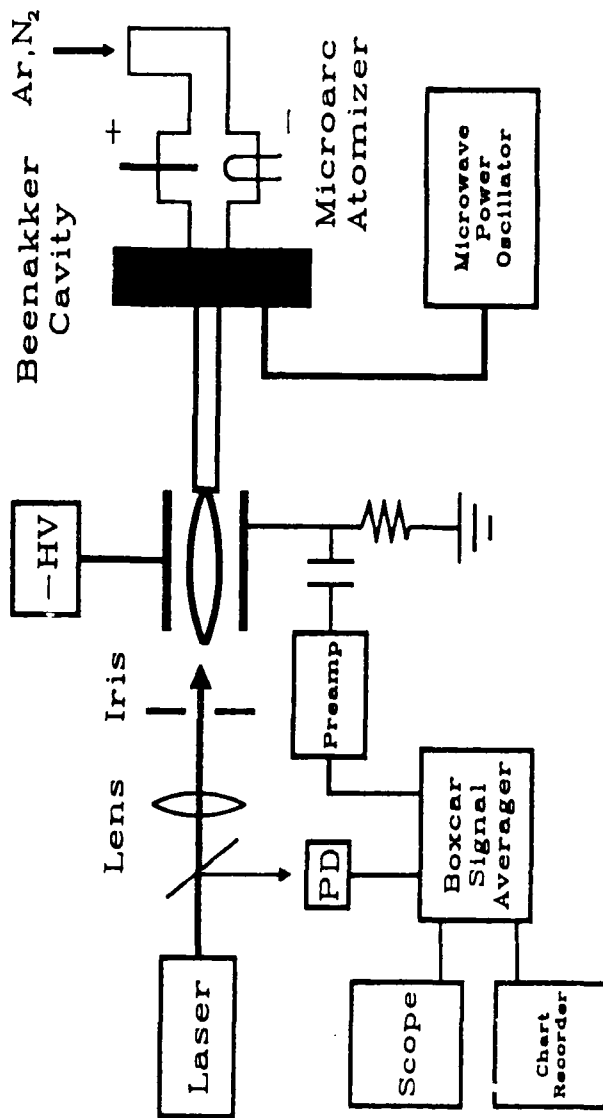
FIGURE CAPTIONS

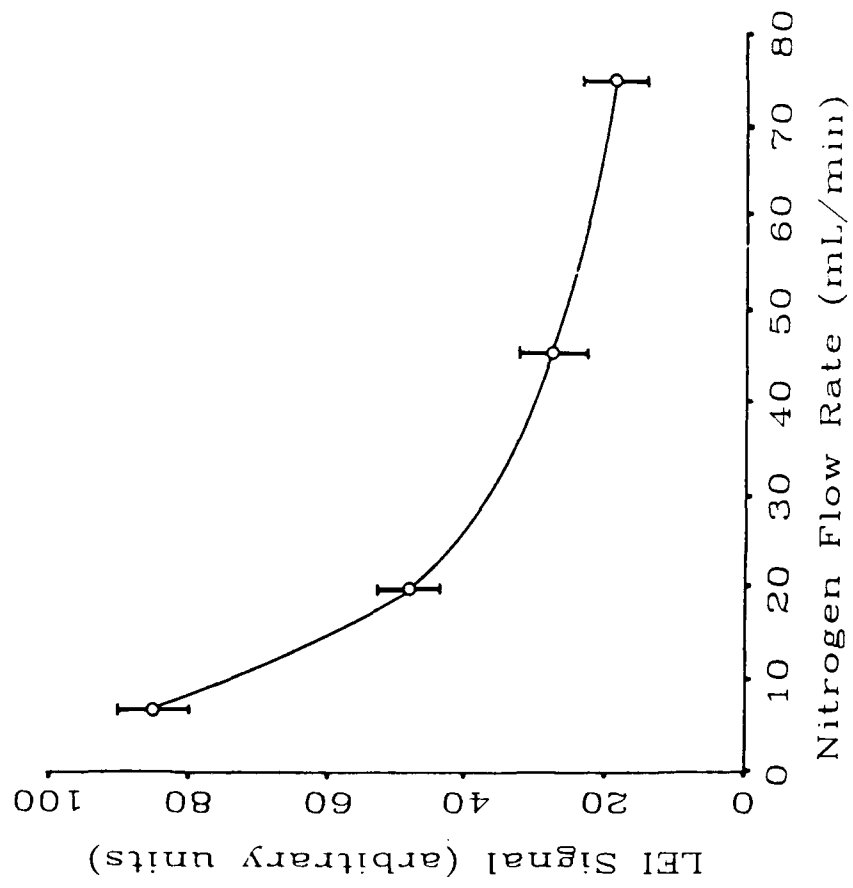
FIG. 1. Schematic diagram of instrumentation. Diode-array spectrometer is omitted.

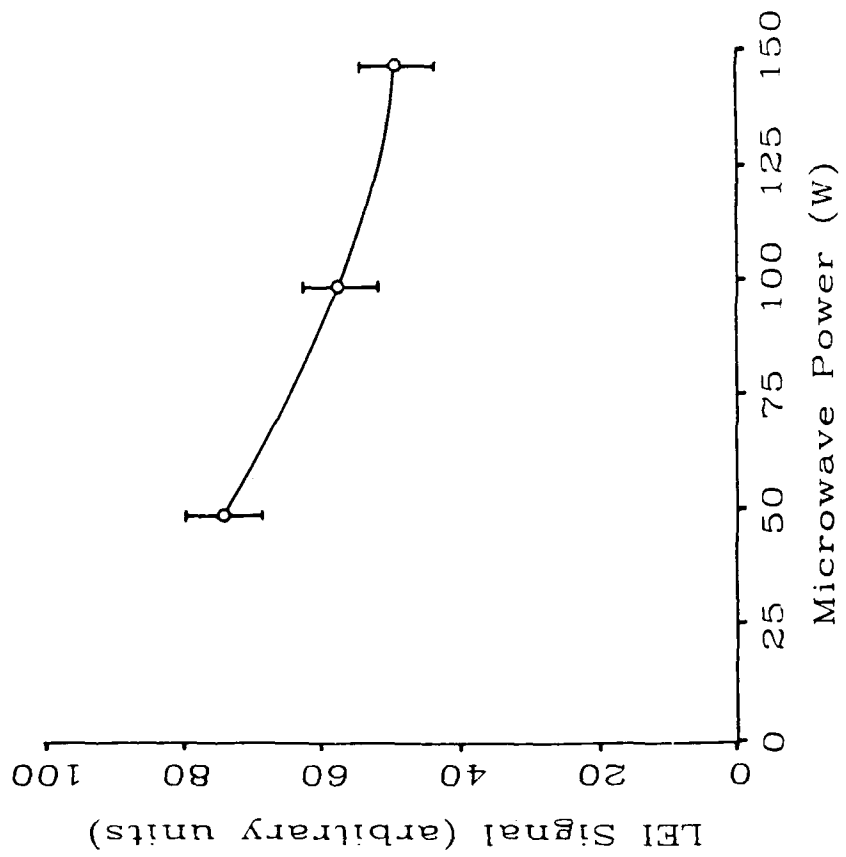
FIG. 2. Effect of nitrogen flow rate on LEI signal for 10 ng indium samples. Error bars represent 95% confidence interval.

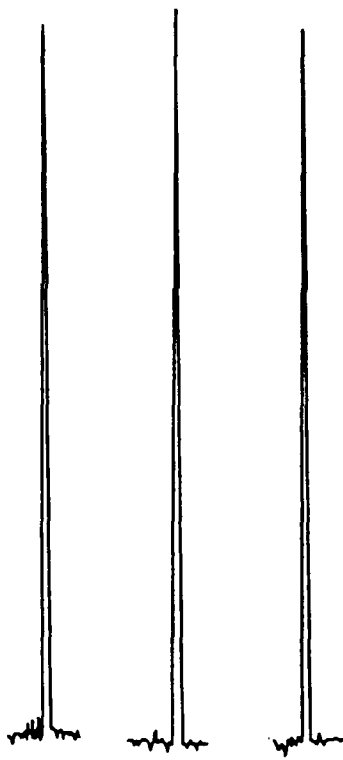
FIG. 3. Effect of microwave power on LEI signal for 10 ng indium samples. Error bars represent 95% confidence interval.

FIG. 4. Chart recorder tracings of consecutive DLI signals for 1 ng indium samples.









LASER-INDUCED IONIZATION SPECTROMETRY: ALTERNATE ATOM RESERVOIRS

Robert B. Green and Michael D. Seltzer
 Chemistry Division, Research Department
 Naval Weapons Center, China Lake, California 93555-6001

Abstract

Premixed flames have been commonly used to atomize samples for laser-induced ionization spectrometry. Detection limits have been excellent but the intrinsic sensitivity of the laser-based methods has been compromised when analyzing real samples. A total consumption flame and several energetic plasmas have been investigated as atom reservoirs for laser-enhanced ionization (LEI) and direct laser ionization (DLI) spectrometry. Ionization from a laser-excited state proceeds by collisions in LEI and absorption of photons in DLI. Laser-enhanced ionization occurs in a flame whenever a laser is tuned to an atomic transition. Whether or not photoionization (i.e., DLI) will supplement the LEI signal depends on the collisional properties of the atom reservoir and the difference between the energy required to reach the ionization potential and the energy of the photoionizing beam. The total consumption flame, active nitrogen, and argon plasmas each have advantages in terms of sample throughput, background, and interferences. The results of LEI and DLI measurements will be used to characterize and compare these atom reservoirs for laser-induced ionization spectrometry.

Introduction

Laser-induced ionization spectrometry may be viewed as a family of techniques (see Figure 1). Laser-enhanced ionization involves thermal or collisional ionization from an excited state that is populated by single-step or stepwise laser excitation.¹ In DLI, sometimes referred to as dual laser ionization,² the final step is laser photoionization. The DLI excitation schemes are similar to those used for resonance ionization spectroscopy (RIS), the distinction being the atom reservoir. Resonance ionization spectroscopy is performed in low pressure atom reservoirs, such as the source of a mass spectrometer. Laser-enhanced ionization and DLI are implemented in atmospheric-pressure plasmas, typically a flame supported by a premix burner. Laser-enhanced ionization and DLI may be viewed as complementary techniques. The former is more well developed but much of the research applies equally well to DLI. Multiphoton ionization (MPI) may also occur in flames but is not useful for trace metal determination. Multiphoton ionization can proceed by the simultaneous absorption of three or more photons of the same wavelength via bound or virtual states. A background signal may result from the MPI of added or native species in the flame, particularly at high incident laser powers. The noise carried by this additive signal can limit minimum detectable concentrations of analytes.

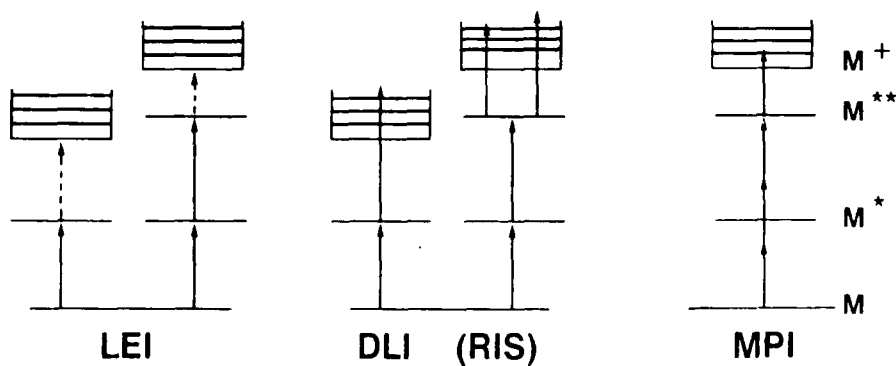


FIGURE 1. Laser-induced ionization schemes: LEI, DLI, and MPI.

Laser-enhanced ionization or DLI may be detected with biased high voltage electrodes inserted in or near the atom reservoir. The increased current in the atom reservoir due to laser excitation is collected, preamplified, and filtered before introduction to a boxcar signal averager. A photodiode which monitors the laser output assures that the signal is sampled only during the laser pulse.

Results and Discussion

The limits of detection for laser-enhanced ionization in premixed flames, compiled and reported in Reference 5, establish the technique as competitive with other high sensitivity analytical methods, such as inductively-coupled plasma emission spectrometry. One component of laser-enhanced ionization spectrometry that might be improved is the atom reservoir. The search for alternate atom reservoirs was driven by the following goals: (1) increasing the analyte residence time in the laser beam, (2) increasing the quantity of analyte in the laser-excited volume, (3) reducing analyte consumption, and (4) further reduction or elimination of electrical interferences. Realistically, it should be recognized that some of these goals may be mutually exclusive.

Total Consumption Flames

One approach to increasing signal is to increase the number of atoms that can be interrogated by the laser beam. This can be accomplished by substituting a total consumption burner for the premixed burner which has been commonly used for LEI spectrometry. In the total consumption burner, the fuel, oxidant, and nebulized sample are not mixed until they exit the burner nozzle. Although 100% of the sample enters the flame, all of it is not available for laser excitation. Large droplets of sample pass through the flame without evaporation. Light scattering from these droplets is the main reason that total consumption burners are no longer used as atom reservoirs for optically-detected spectrometry. Since an electrical current is measured directly in LEI spectrometry, light scattering causes no detection problems. Even though a portion of the sample is lost to LEI, the overall increase in sample throughput over the premixed burner which rejects 95% of the aspirated sample led to a net improvement in limits of detection for the elements studied.⁶ An additional benefit of using the total consumption burner is the availability of oxygen-based flames without the threat of explosive flashback.

Laser-enhanced ionization spectrometry with a total consumption burner has some disadvantages as well. When compared with the premixed burner, the laser pathlength for the total consumption burner is reduced because the flame has a circular cross-section. Because the flame is very turbulent, the concentration gradient is diffuse and the zone of highest concentration is not well defined. The high sample throughput, the central advantage of the total consumption burner, leads to two problems: MPI background and the earlier onset of electrical interferences. The origin of the background is the MPI of flame species produced by the aspiration of water, the primary solvent for this work. The largely featureless MPI background occurs only at high incident laser powers. Since the MPI background signal was additive, it was possible to subtract it, but the random noise carried by the MPI remained. The strategy to obtain the best detection limits was to increase the laser power until MPI was observed. Then the laser power was reduced slightly below the MPI level and the detection limits were determined in the absence of MPI noise. The appearance of MPI background is also possible with a premix burner; the difference is that most of the solvent is eliminated by condensation before it reaches the flame. The earlier onset of electrical interferences due to easily-ionized species with the total consumption burner is also a symptom of the "100%" sample introduction into the flame. The actual flame concentration (or density) of ions when signal suppression occurs is probably the same for both burners. The difference is that this flame concentration occurs at much lower solution concentrations of the interferent when using a total consumption burner. It is the absolute flame concentration of interferent that determines the level of LEI signal suppression not the ratio of interferent to analyte.⁷

Sample Desolvation

Sample desolvation prior to introduction was one approach to attacking the deficiencies of the total consumption burner. Sample desolvation has long been used in atomic spectrometry but the reported sample transport efficiencies for available techniques were low. Less than complete sample transport negates the value of using a total consumption burner.

A successful approach involved using a graphite furnace to desolvate the sample prior to introduction into the total consumption burner.⁸ The liquid sample was deposited in the graphite tube, the water was driven off in a drying cycle, and the sample was atomized into a flowing stream of argon. The gas-phase sample was carried into the aspiration tube of the burner. A water vapor generator was connected in the gas line from the furnace for comparison of the introduction of dry and wet samples into the total consumption burner. Wet samples could not be introduced directly from the furnace because spattering would cause sample loss making the results equivocal.

The advantages of sample desolvation are illustrated in Figure 3. Five trials are shown. In the three trials where the manganese sample was desolvated, sharp signal peaks result. The MPI background yields a DC signal offset for the two trials with solvated samples. The increased noise carried by the signal is obvious. The reduction of peak amplitudes in the solvated trials is probably due to the cooling of the flame by water vapor introduction, thereby reducing the analyte atom fraction.

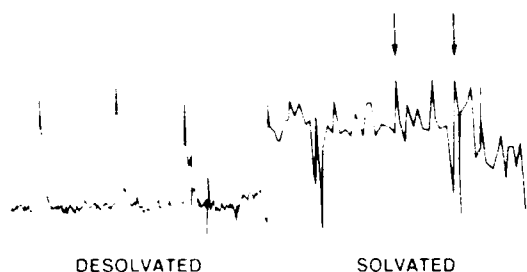


FIGURE 3. Comparison of signals for desolvated and solvated Mn samples. The arrows indicate signals for the solvated samples.

In summary, sample desolvation with the total consumption burner provides many advantages that are applicable to laser-induced ionization spectrometry.⁸ Higher laser powers can be effectively used to saturate atomic transitions. It is also possible to condense the total consumption flame by introducing it into a Vycor tube. The exciting laser beam may then be directed down the length of the flame and longer pathlength electrodes may be used. Flame condensation and pathlength extension can be applied to the total consumption flame without sample desolvation but the increased MPI noise nullifies any improvements in signal. Finally, intrinsic flame temperatures are maintained by the removal of aqueous solvents. All of these advantages lead to order-of-magnitude improvements in detection limits for laser-enhanced ionization spectrometry using total consumption burners with sample desolvation.⁸

Energetic Plasmas

Recently, microwave-induced plasmas have been investigated as atom reservoirs for laser-induced ionization. The apparatus is shown in Figure 4. The gas for plasma formation is directed through the sample introduction device. Several sample introduction devices have been used: an AC microarc, ultrasonic nebulization with solvent stripping, and a graphite furnace. The sample vapor is then carried through the microwave cavity where the plasma is generated. All of this research has involved atmospheric pressure plasmas. The plasma is conducted beyond the microwave cavity with a quartz tube. Signal collection and processing are similar to the approach used in flames.

The first plasma to be investigated was active nitrogen.⁹ Active nitrogen has interesting energetic properties and is capable of efficiently producing excited metal atoms and ions on collision with ground state species. The metal emission in sub-atmospheric pressure sources has been detected photoelectrically for analytical determinations.¹⁰ The active nitrogen in the present work was generated by adding molecular nitrogen to an argon flow in about a 1- to 10 ratio. Microwave powers in the range from 50 to 150 W were used.

Both LEI and DLI experiments were run to evaluate the collisional properties of active nitrogen. The excitation schemes for indium are shown in Figure 5. Laser-enhanced ionization occurs in a plasma whenever a laser is tuned to an atomic transition. For otherwise identical experiments, the enhancement of the DLI signal over LEI depends on the collisional environment of the plasma and how well the energy of the photon matches the energy required for photoionization. In this case, the energy overshoot was 0.34 eV.

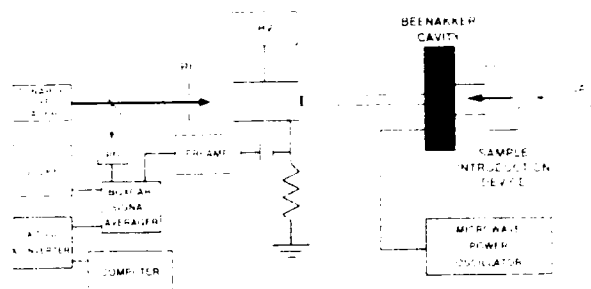


FIGURE 4. Schematic diagram of instrumentation for laser-induced ionization spectrometry in a microwave-induced plasma.

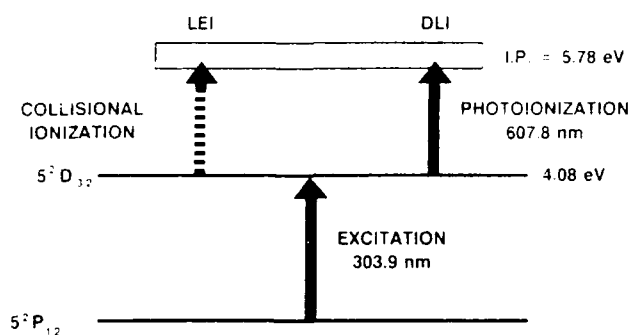


FIGURE 5. LEI vs. DLI for indium.

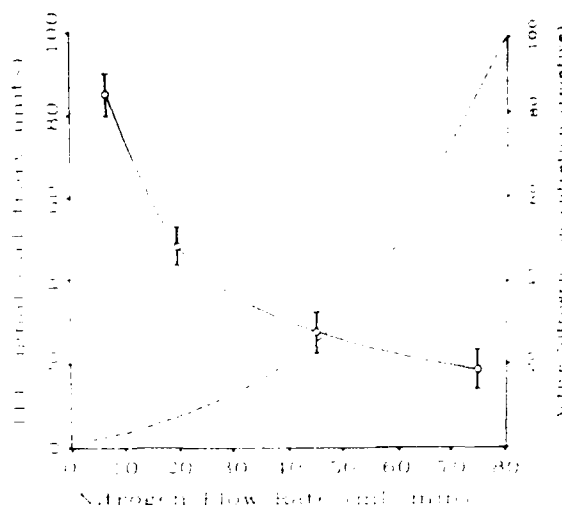


FIGURE 6. LEI and active nitrogen dependence on nitrogen flow rate.

A detection limit for DLI of indium was estimated to be 20 pg. The DLI signal was a factor of two larger than the LEI signal. Since the energy overshoot was relatively small for the photoionizing wavelength, the collisional properties of active nitrogen were judged to be good although perhaps not comparable to an air-acetylene flame.

During the optimization of the laser-induced ionization processes, some interesting signal behavior was noted. Figure 6 illustrates the results of experiments in which the LEI signal was monitored while increasing the nitrogen flow rate. As expected, the active nitrogen concentration (broken line) increased as the nitrogen flow rate was increased. The decrease in LEI signal was not expected. It was first speculated that the laser excitation prior to the signal collection region could be significantly depleting the ground state atom population. On further consideration, it seemed unlikely that a major signal suppression was caused by a relatively minor loss of atoms. Experiments in which atomic fluorescence was measured for identical concentrations of lead in both the pure argon plasma and the active nitrogen plasma (i.e., nitrogen in argon) gave essentially identical limits of detection. This suggested that quenching of the excited state analyte played a very minor role in the signal suppression observed at high nitrogen flows. Current vs. applied voltage curves (slope = $1/R$) for air-acetylene flames (sodium-seeded and unseeded) were compared with similar curves for active nitrogen and pure argon plasmas. The behavior of the sodium-seeded flame and active nitrogen plasma was very similar, suggesting that the signal suppression observed as the nitrogen flow rate was increased was due to the formation of a space charge at the electrodes. This was somewhat surprising because the currents in the active nitrogen plasma were up to two orders-of-magnitude lower than currents measured in the air-acetylene flame.

Investigations of laser-induced argon plasmas have also been initiated. Preliminary results suggested that space charge formation in argon was minimal. The laser-induced ionization background was low and featureless in the wavelength region of interest. (The active nitrogen laser-induced ionization spectrum has been characterized from 279 to 285 nm.¹¹) Because of the low background, manganese has been detected at the tens of picogram levels. No suppression of the manganese signal was observed in signal recovery experiments using sodium as an interferent over a two order-of-magnitude concentration range. Electrical breakdown occurs at a lower applied voltage in argon than active nitrogen meaning that signal collection voltages will be limited.

Conclusions

The total consumption burner has been demonstrated as a viable atom reservoir for laser-induced ionization spectrometry but further research must be undertaken before these results can be translated into practice. Energetic plasmas present some interesting possibilities. Because of its good collisional properties and long lifetime, active nitrogen plasmas may be incorporated into an interferent removal scheme.¹² Easily-ionized species could be

removed with biased electrodes prior to laser-induced ionization. Preliminary experiments with microwave-induced argon plasmas have suggested that it may be an attractive alternative to flames because of its low background and the apparent absence to electrical interferences.

Acknowledgment

In addition to the authors, many people have contributed to the body of research that is presented here. Many of them are represented in the references.

References

1. J. C. Travis, G. C. Turk, and R. B. Green, *Anal. Chem.* 54, 1006A (1982)
2. C. A. Van Dijk, F. M. Curran, K. C. Lin, and S. R. Crouch, *Anal. Chem.* 53, 1275 (1981)
3. G. C. Turk, *Anal. Chem.* 53, 1187 (1981)
4. J. D. Messman, N. E. Schmidt, J. D. Parli, and R. B. Green, *Appl. Spectrosc.* 39, 504 (1985)
5. G. C. Turk, *J. Anal. Atom. Spec.*, 2, 573 (1987)
6. M. A. Nippoldt and R. B. Green, *Anal. Chem.* 55, 554 (1983)
7. J. E. Hall and R. B. Green, *Anal. Chem.* 55, 1811 (1983)
8. J. E. Hall and R. B. Green, *Anal. Chem.* 57, 431 (1985)
9. M. D. Seltzer and R. B. Green, *Spectrosc. Letters*, 20, 601 (1987)
10. T. M. Niemczyk and H. C. Na, *Appl. Spectrosc. Rev.*, 19, 363 (1983)
11. M. D. Seltzer, E. H. Piepmeier, and R. B. Green, *Appl. Spectrosc.*, submitted
12. T. O. Trask and R. B. Green, *Spectrochim. Acta*, 38B, 503 (1983)

OPTOGALVANIC SPECTROSCOPY IN A MICROWAVE-INDUCED
ACTIVE NITROGEN PLASMA

M. G. Seltzer,* E. H. Piepmeier, and R. B. Green
Chemistry Division, Research Department, Naval Weapons Center,
China Lake, CA 93555 (M.G.S. and R.B.G.) and Department of Chemistry,
Oregon State University, Corvallis, OR 97331 (E.H.P.)

ABSTRACT

Optogalvanic spectra have been obtained for a microwave-induced active nitrogen plasma. The spectra originated from laser-excited transitions belonging to the second positive system of nitrogen. As the ultraviolet (UV) laser wavelength was scanned through the regions of interest, the laser-induced ionization signal was monitored. A laboratory-constructed etalon system of very low finesse was used to provide an interferometric wavelength reference. Calibration of the laser wavelength allowed the accurate identification of a series of selected nitrogen transitions.

Index Headings: Optogalvanic Spectroscopy, Laser-Induced Ionization,
Active Nitrogen

INTRODUCTION

Laser-induced optogalvanic spectroscopy is a simple, yet powerful technique for obtaining high-resolution excitation spectra for atoms and molecules in electrical discharges.¹ Optogalvanic signals are generated by impedance changes that occur in response to the absorption of laser radiation by atomic and molecular species within the discharge.² Optogalvanic spectroscopy is characterized by highly efficient signal collection and, because electric current rather than light is detected, one does not have to contend with discriminating against background emission or scattered source radiation. In this respect, optogalvanic detection provides some advantages over laser-induced fluorescence techniques.

Following the initial report by Green et al.,¹ of galvanic detection of optical absorptions in a gas discharge, there have been numerous applications of optogalvanic spectroscopy for the study of molecules in a variety of discharges. Feldmann³ reported an optogalvanic study of NH_2 , NO_2 , H_2 , and N_2 in an electrical discharge. Changes in the discharge voltage were monitored as the laser wavelength was scanned through several visible transitions of the molecular species of interest. The author observed that the region of the discharge selected for illumination was critical for obtaining a high ratio of signal-to-background. Suzuki et al.,^{4,5} have carried out optogalvanic spectroscopy of nitrogen in a radio frequency (RF) discharge by using a resonant tank circuit to monitor changes in the discharge current. They obtained high-resolution spectra for transitions to Rydberg states of nitrogen.⁵ Suzuki et al.,⁵ have also carried out similar studies in a low pressure

microwave discharge. Miyazaki et al.,^{7,9} reported double resonance optogalvanic spectroscopy of nitrogen in hollow cathode discharges. This state-selective method allowed the recording and assignment of new visible bands. Several infrared optogalvanic studies of molecular species have also been reported.³⁻¹²

Laser-induced optogalvanic spectroscopy has been used to study molecular species in flames as well as discharges. Schenck et al.,¹³ recorded the absorption spectra of metal oxides in flames using optogalvanic detection. The metal oxides were obtained by aspirating metal salt solutions into a pre-mixed air/hydrogen flame. Mallard et al.,¹⁴ Cool,¹⁵ and Rockney et al.,¹⁶ have carried out multiphoton ionization for optogalvanic detection of NO in flames. Cool and Goldsmith¹⁷ have recently reported a laser-enhanced flame ionization chromatographic detector for hydrocarbons. For a more complete overview of the literature of optogalvanic spectroscopy, the reader is referred to reviews by Webster and Rettner² and Goldsmith and Lawler.¹⁸

Active Nitrogen Plasma. Microwave-induced plasmas employing both atomic and molecular gases are commonly used as sources for atomic emission spectrometry.¹⁹ The active nitrogen plasma is unique among these plasmas in terms of its energetics and the presence of metastable species.²⁰ In the active nitrogen plasma, diatomic nitrogen molecules exist in a variety of electronic, vibrational, and rotational excited states.²¹ The active nitrogen plasma is an efficient excitation source because of its ability to collisionally transfer up to several electron volts of energy to analyte species in the plasma.²²

Recently, we investigated a microwave-induced, active nitrogen plasma as a potential atom reservoir for laser-induced ionization spectrometry.²³ Laser-induced ionization²⁴ includes direct photoionization and laser-enhanced collisional ionization. (The latter has been referred to as the optogalvanic effect in flames.) The active nitrogen plasma was investigated as an alternative to the flame, which has been the traditional atom reservoir for laser-induced ionization spectrometry. In the course of that investigation, a background ionization signal was detectable in the absence of analyte in the plasma, even at low laser irradiance. With increased UV laser irradiance of the plasma, a highly structured background spectrum was revealed, corresponding to the second positive band system of nitrogen. The second positive system originates from electronic transitions that exist several electron volts above the ground state but are commonly observed by emission in low pressure electrical discharges in nitrogen.²⁵ The observation of these transitions in this laboratory prompted further investigation of the laser-induced background ionization of the active nitrogen plasma.

The study of dense spectra, such as that generated in a molecular discharge, typically requires the high spectral resolution afforded by emission spectrographic techniques. The long focal length monochromators used to provide the necessary resolution, do so at the expense of light throughput and consequent loss of sensitivity. Laser-induced optogalvanic techniques are characteristically well suited for the study of dense spectra in radiating plasmas, where conventional optical methods demonstrate only limited sensitivity.⁷ The high photon flux and spectral selectivity of a laser, coupled with the high signal collection efficiency of the electrical detection system provide a useful alternative to traditional emission techniques.

The majority of published results of optogalvanic studies of molecules have involved the use of visible or infrared laser sources. The present paper reports for the first time, a UV optogalvanic study of a microwave-induced, atmospheric pressure active nitrogen plasma. The existence of significant excited state populations in the active nitrogen plasma, in addition to the availability of high UV laser irradiance, allowed the recording of high resolution, excited-state excitation spectra. The spectra of representative portions of the second positive system of nitrogen were observed by detecting the laser-induced ionization while scanning the laser wavelength, using a frequency doubler with autotracking capability. Simultaneous interferometric calibration of the laser wavelength permitted the accurate identification of a series of excitation peaks in this band system.

The information obtained from an optogalvanic study of the active nitrogen plasma is valuable in terms of its relevance to laser-induced ionization spectrometry carried out in the plasma. Detailed knowledge of the plasma background facilitates the selection of analyte excitation lines and is an asset in obtaining optimum signal-to-background ratios and, hence, greater sensitivity.

EXPERIMENTAL SECTION

The microwave-induced, atmospheric pressure active nitrogen plasma used for this study was the same as that used in Ref. 23. For the present study, the plasma was operated with an applied microwave power of 70 W with reflected power less than 10 W. A mixture of argon and nitrogen with flow rates

1.2 L/min and 50 mL/min respectively, sustained the plasma. The pure nitrogen was obtained from liquid nitrogen boil-off and the argon used was high purity grade 99.995% from Matheson. These gas sources were selected to minimize introduction of O_2 , NO , and water vapor into the plasma. The argon discharge that was generated did not extend beyond the immediate vicinity of the microwave cavity. The metastable nitrogen plasma, however, propagated several centimeters downstream from the discharge and formed a converging plasma plume at the end of the quartz flow tube. The role of the argon in generating the active nitrogen is not well understood although it is possible that energy is transferred between argon plasma species and ground state nitrogen molecules. In the absence of nitrogen in the plasma, only a featureless, wavelength-independent signal was detected for excitation of argon over the region of study. There was no indication of signals originating from argon transitions with nitrogen present in the plasma.

A Nd:YAG pumped dye laser (model 581-C/TDL50, Quantel) with frequency doubling and autotracking capability was used for all experiments. The laser was operated at 10 Hz with rhodamine 590 tetrafluoroborate (Exciton). The UV output pulsewidth and bandwidth of the laser were specified by the manufacturer to be 6-8 ns and 0.003 nm, respectively.

Detection System. The detection system for the optogalvanic study of the active nitrogen plasma was the same as that used in Ref. 23 for laser-induced ionization spectrometry. The active nitrogen plasma plume was illuminated along its longitudinal axis in the same manner as in Ref. 23. A pair of molybdenum plate electrodes (12-mm x 60-mm) were positioned symmetrically about the plasma plume, 8 mm apart. A 5-mm diameter iris was used to prevent

the laser beam from striking the electrodes in order to minimize photoelectric emission. A potential of -1500 V was applied to the cathode using a highly regulated power supply (model 229, Pacific Instruments). The anode circuit consisted of a 10 K load resistor, a 500 pF blocking capacitor, and a preamplifier.²⁶ The pulsed ionization signals were processed with a boxcar averager (model 162, Princeton Applied Research) with a model 165 gated integrator module. A 1- μ s boxcar aperture was used to sample the ionization pulse. An effective time constant of 0.1 s was chosen because it produced the least distortion of the spectra as the laser wavelength was scanned at a nominal rate of 0.025 $\text{\AA}/\text{s}$. A 5- μ s high pass filter was used between the preamplifier and boxcar to attenuate low frequency noise. The boxcar output signal was recorded on one channel of a digital oscilloscope (model 4094, Nicolet).

Wavelength Calibration. Mechanical flaws in the sine bar drive of the dye laser grating can cause discrepancies between the actual output wavelength and that indicated by the laser readout display.¹⁴ Similar behavior was observed for the laser used in the present work. This necessitated the use of an external calibration system. Accurate wavelength identification was obtained by simultaneously recording on a second channel of the digital oscilloscope the sinusoidal interference signal from the reflections of an uncoated, 3.3-mm thick silica etalon. Figure 1 illustrates the interferometer configuration. The beams reflected from the front and back surfaces of the etalon combined to produce interference fringes, one of which was monitored through a pinhole by a photodiode. The pinhole was placed in the most intense region of the interference pattern. The output signal from the photodiode was processed with a second boxcar averager prior to recording with the digital oscilloscope.

The dye laser used for this work employs a prism output separator to dispersively separate the second harmonic UV output from the fundamental beam. Ordinarily, the fundamental beam is directed to a beam dump. For the present application, the visible beam was conveniently available and was used for wavelength calibration to avoid distorting the UV beam and reducing its intensity. Wavelengths in the visible region determined in this manner were divided by 2 to obtain the corresponding UV wavelengths.

As the laser wavelength was scanned, the sinusoidal modulation of the intensity of the reflected interference fringes was monitored at the photodiode. The pattern was similar to that typically produced by a very low finesse Fabry-Perot interferometer. Monitoring of the transmitted interference pattern from a high finesse etalon is more common. Monitoring the low finesse transmitted pattern produces a sinusoidal type modulation that varies from maximum to about 92% of maximum. A large zero-offset would be required for photoelectric detection of this signal, and the signal would be relatively noisy. However, the reflected interference pattern for a low finesse Fabry-Perot interferometer produces a more easily recorded high-contrast sinusoidal type modulation that varies from maximum to near zero intensity.

Constructive interference occurs when the beam reflected from the back surface of the etalon is in phase with the beam reflected from the front surface. This occurs²⁷ for an etalon that is slightly off axis when

$$\lambda_{\text{air}} = \frac{2t}{mn_1} (n_2^2 - n_1^2 \sin^2\theta)^{1/2} \quad (1)$$

where m is the order of the etalon (an integer, typically around 17,000), λ_{air} is the laser beam wavelength in air, t is the physical thickness of the etalon (same units as λ_{air}), n_1 is the refractive index of the etalon at λ_{air} , n_2 is the refractive index of air at λ_{air} and θ is the angle between the laser beam and the normal to the etalon surfaces. The refractive indices were computed using the equations in Ref. 27.

The value for θ was determined from the positions of the incident and reflected beams. The values for m and t were obtained by iterating m in the following manner. First, the interferometer was calibrated by using laser-enhanced ionization in an air-acetylene flame to detect known spectral lines. The wavelength region containing these lines was scanned while simultaneously recording the sinusoidal interference pattern (as was done for all scans). In the sinusoidal interference pattern, a peak of maximum intensity was arbitrarily assigned the integer order M (having as yet an unknown value). This was called the reference order. Two of the spectral lines were chosen, one near each end of the scan. The exact number (including fraction), ΔM_i , of sinusoidal cycles from the reference order to each spectral line, i , was measured. For each spectral line, $M + \Delta M_i$ was used for m in Equation 1 since each cycle corresponds to one order change. Both these equations were then solved for t and the integer M was iterated until the predicted values of t for the two wavelengths were closest to each other. Then the value of t for the line closest to the reference order was used with Equation 1 to calculate the wavelength of any new line. In the latter calculation, an iterative method was used to calculate the wavelength because the refractive indices are functions of wavelength.

The choice of spectral lines and conditions to calibrate the laser are important to obtain accurate results. Spectral lines should be chosen whose wavelengths are accurately known and whose spectral profiles are symmetrical. This avoids uncertainty in locating the center of the line profile as the center was presumably used when the wavelength tables were originally generated. It is also important to avoid optical saturation, prefilter absorption (and postfilter absorption if fluorescence detection is used), which can unnecessarily broaden and often distort the spectral profile.²⁹ Often a compromise must be made between a line that does not show such distortions, yet provides a strong enough signal to be useful. The Co lines at 279.706 and 279.377 nm were used to calibrate the interferometer because they were in the wavelength region of interest, symmetrical, and not distorted.

RESULTS AND DISCUSSION

Optogalvanic spectra for nitrogen were recorded for the wavelength region between 279.00 and 283.00 nm in increments of 0.85 nm per scan. The corresponding sinusoidal interference signal was simultaneously recorded. Figures 2 and 3 show these excitation spectra with approximate wavelength scales. Note the 0.05-0.10 nm overlap between consecutive spectra. The spectra presented here were not normalized for laser intensity. The average power of the second harmonic output of the laser was 35 mW and was maintained within 10% of this value for all scans.

The interferometer was calibrated in the manner described above. For each recorded scan, the positions of the major spectral features were accurately noted by using the vertical cursor of the digital oscilloscope. The corresponding interferometer order (including fraction) was also noted. These values were tabulated using an electronic spreadsheet (Lotus 1-2-3, Lotus Development Corp.). The wavelength of each peak was calculated using the calibration factors that were previously determined for the interferometer. These wavelength assignments were re-tabulated and compared to peak assignments published by Von Rutenbender and Herzberg²⁵ for optically detected emission from the second positive system of nitrogen in a low pressure electrical discharge. Emission bands corresponding to the second positive system actually range from 200 nm to 500 nm.²² The nitrogen second positive system consists of transitions between vibrational states in the $C^3\Pi_u$ and $B^3\Pi_g$ electronic levels of nitrogen. The spectra shown in Fig. 2 include transitions between vibrational states 3+0 and 4+1. The individual peaks that make up the spectra in Figs. 2 and 3 represent transitions originating from and terminating at specific rotational states within the respective vibrational states.

The optogalvanic excitation spectrum shown in Fig. 4 was recorded between 280.00 and 280.85 nm and was selected for calibration and wavelength assignment. The majority of the peaks in Fig. 4 are well resolved with full widths at half maximum of 0.006 nm or less. It is possible that some of the broader peak profiles may be the result of distortion due to overlap with peaks of the same or other band systems.³ For the spectral region between 280.00 and 280.85 nm, wavelength assignments were obtained for 32 peaks. These peaks were the most easily distinguishable and represent only a fraction of the one

hundred or so reported transitions for the spectral region between 890.000 and 910.000 cm⁻¹. The calculated assignments for these lines are listed in Table I along with the literature value²⁵ and calculated differences. All wavelength assignments were within 0.018 nm of the published values.

The observation of individual peaks depends on the population of the rotational state from which the transition originates and the ability of the instrument to resolve that peak from adjacent peaks. The population of the various rotational states of nitrogen is a function of the temperature of the plasma, and therefore, many transitions may not be observed under a given set of plasma operating conditions. The resolution of the technique is limited by a number of factors. Spectral broadening mechanisms within the plasma may cause overlap of adjacent lines. This factor may be addressed by employing Doppler-free intermodulation techniques⁵ and also by working in a low pressure active nitrogen plasma. Narrowing the laser bandwidth may also improve the resolution.

CONCLUSION

An optogalvanic spectroscopic study of a microwave-induced active nitrogen plasma has been carried out. Recordings of portions of the optogalvanic spectrum of the nitrogen second positive system demonstrate that several of the transitions that are routinely observed in a nitrogen electrical discharge by emission techniques can also be observed by laser-induced ionization of an active nitrogen plasma. The conspicuous absence of several peaks indicates that the population of various rotational states in excited

electronic levels of nitrogen varies between different types of discharges. Additional detailed information regarding the electrical discharge used in Ref. 23 would be required for a direct comparison between that discharge and the plasma described in the present paper. Since the population of rotational states in a given type of discharge is a function of temperature, cathodoluminescence spectroscopy may provide a useful diagnostic tool for plasma temperature measurement.

The present work provides useful information concerning the laser-induced ionization background of the active nitrogen plasma. The spectral region chosen for this study overlaps several atomic lines commonly used for laser-induced ionization spectrometry.²⁴ The detection and calibration techniques described here can easily be used to explore transitions in other wavelength regions as well. The spectral mapping obtained in the present study provides a means by which optimum analytical lines can be selected or background-limited lines can be avoided.

ACKNOWLEDGMENT

Michael D. Seltzer and Edward H. Piepmeier gratefully acknowledge the Office of Naval Technology and the American Society for Engineering Education for postdoctoral fellowship support (M.D.S.) and summer faculty fellowship support (E.H.P.).

REFERENCES

1. R. S. Green, R. A. Keller, G. S. Luther, P. K. Schenck, and J. C. Travis, *Appl. Phys. Lett.* **29**, 747 (1976)
2. J. P. Webster and C. T. Rettner, *Laser Focus Rep.*, **9** (1980)
3. D. Felmann, *Opt. Commun.* **29**, 67 (1979)
4. T. Suzuki, *Opt. Commun.* **38**, 364 (1981)
5. T. Suzuki and M. Kakimoto, *J. Mol. Spectrosc.* **93**, 423 (1982)
6. T. Suzuki, H. Sekiguchi, and T. Kasuya, *J. de Physique, Colloque C7 44*, 419 (1983)
7. K. Miyazaki, H. Scheingraber, and C. R. Vidal, *Phys. Rev. Lett.* **50**, 1046 (1983)
8. C. R. Webster and R. T. Menzies, *J. Chem. Phys.* **78**, 2121 (1983)
9. K. Miyazaki, H. Scheingraber, and C. R. Vidal, *J. de Physique, Colloque C7 44*, 411 (1983)
10. C. R. Webster and R. T. Menzies, *Proc. SPIE-Int. Soc. Opt. Eng.* **438**, 152 (1983)
11. C. Hameau, J. Wascot, D. Dangoisse, and P. Glorieux, *Opt. Commun.* **49**, 423 (1984)
12. S. W. Kim and W. E. Jones, *Spectrosc. Lett.* **18**, 767 (1985)
13. P. K. Schenck, W. G. Mallard, J. C. Travis, and K. C. Smyth, *J. Chem. Phys.* **69**, 5147 (1978)
14. W. G. Mallard, J. H. Miller, and K. C. Smyth, *J. Chem. Phys.* **76**, 3433 (1982)
15. T. A. Cool, *Appl. Optics* **23**, 1559 (1984)

16. B. H. Rockney, T. A. Cool, and E. R. Grant, Chem. Phys. Lett. **87**, 141 (1982)
17. T. A. Cool and J. E. M. Goldsmith, Appl. Opt. **26**, 2542 (1987)
18. J. E. M. Goldsmith and J. E. Lawler, Contemp. Phys. **22**, 135 (1981)
19. A. T. Zander and G. J. Hieftje, Appl. Spectrosc. **35**, 657 (1981)
20. A. W. Jolant and C. A. Winkler, Active Nitrogen, Academic, New York (1968)
21. J. T. Clay and T. M. Niemczyk, Spectroscopy, **2(8)**, 36 (1987)
22. T. M. Niemczyk and H. C. Na, Appl. Spectrosc. Rev. **19**, 363 (1983)
23. M. D. Seltzer and R. B. Green, Spectrosc. Lett. **20**, 601 (1987)
24. J. C. Travis, G. C. Turk, and R. B. Green, Anal. Chem. **54**, 1006A (1982)
25. Von G. Bittenbender and G. Herzberg, Annal. der Physik. **5(21)**, 577 (1934/35)
26. G. J. Havrilla and R. B. Green, Chem. Biomed. and Environ. Instr. **11**, 273 (1981)
27. G. J. Beenen, J. W. Hosch, and E. H. Piepmeier, Appl. Spectrosc. **35**, 593 (1981)
28. E. H. Piepmeier and G. J. Beenen, Appl. Spectrosc. **36**, 235 (1982)

TABLE I

Peak number	Observed wavelength (nm)	Literature* wavelength (nm)	Wavelength difference (nm)
(1)	280.768	280.768	0.000
(2)	280.270	280.273	-0.003
(3)	280.283	280.280	0.003
(4)	280.286	280.289	-0.003
(5)	280.294	280.291	0.003
(6)	280.334	280.337	-0.003
(7)	280.342	280.346	-0.004
(8)	280.373	280.370	0.003
(9)	280.392	280.393	-0.001
(10)	280.409	280.409	0.000
(11)	280.425	280.425	0.000
(12)	280.445	280.446	-0.001
(13)	280.462	280.460	0.002
(14)	280.480	280.481	-0.001
(15)	280.514	280.510	0.004
(16)	280.544	280.544	0.000
(17)	280.576	280.568	0.008
(18)	280.605	280.603	0.002
(19)	280.633	280.627	0.006
(20)	280.643	280.639	0.004
(21)	280.658	280.662	-0.004
(22)	280.675	280.680	-0.004
(23)	280.684	280.691	-0.007
(24)	280.708	280.707	0.001
(25)	280.731	280.732	-0.001
(26)	280.751	280.746	0.005
(27)	280.771	280.776	-0.005
(28)	280.789	280.789	0.000
(29)	280.802	280.799	0.003
(30)	280.808	280.811	-0.003
(31)	280.823	280.823	0.000
(32)	280.838	280.835	0.003

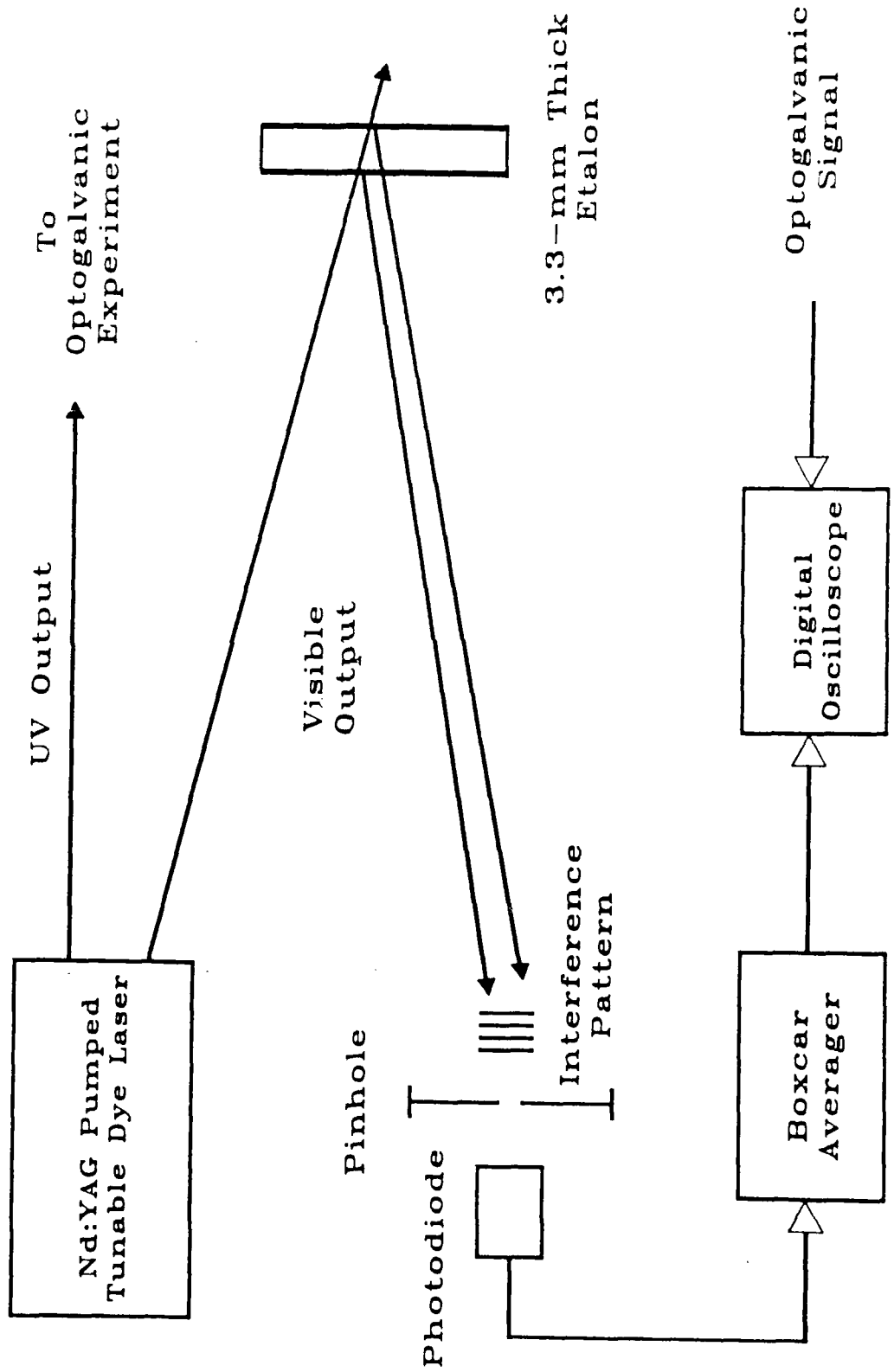
* See Ref. 25.

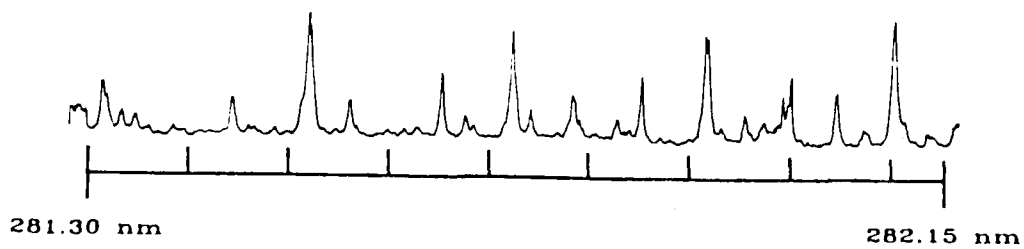
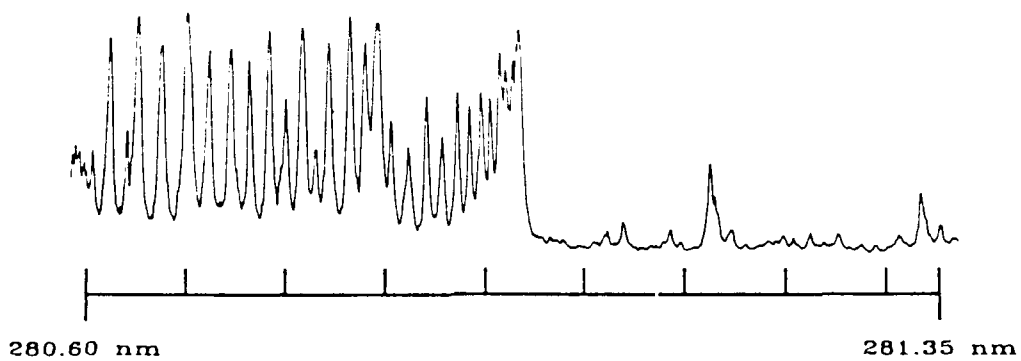
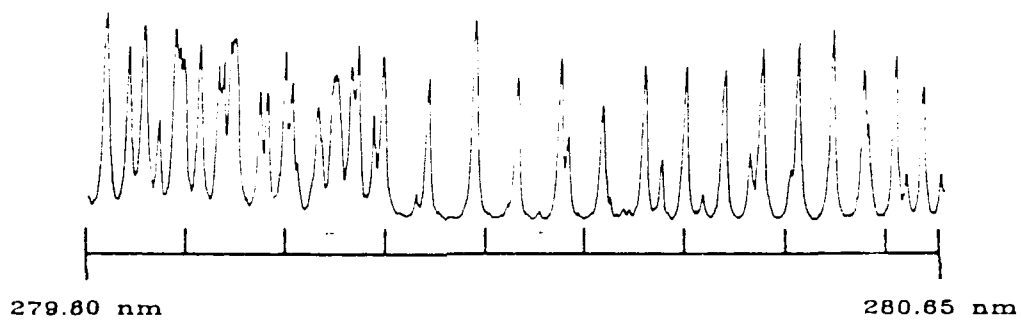
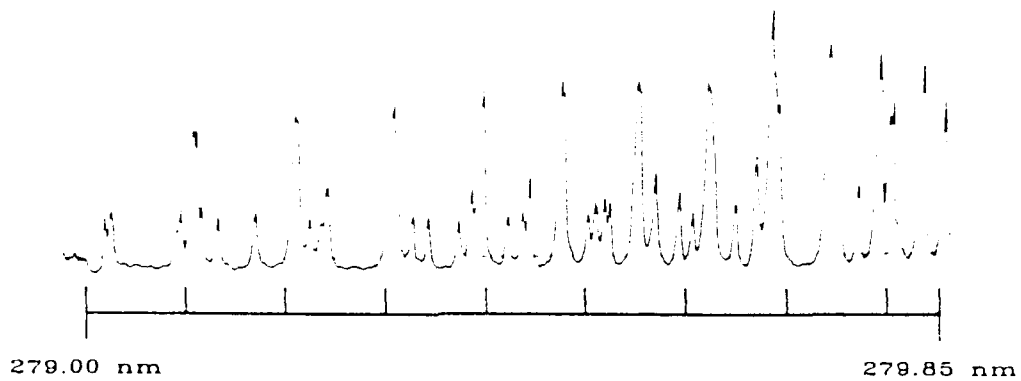
Figure Captions

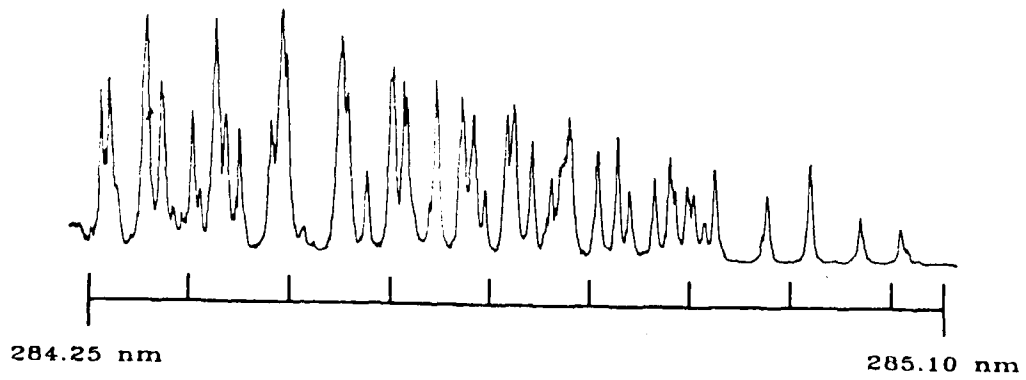
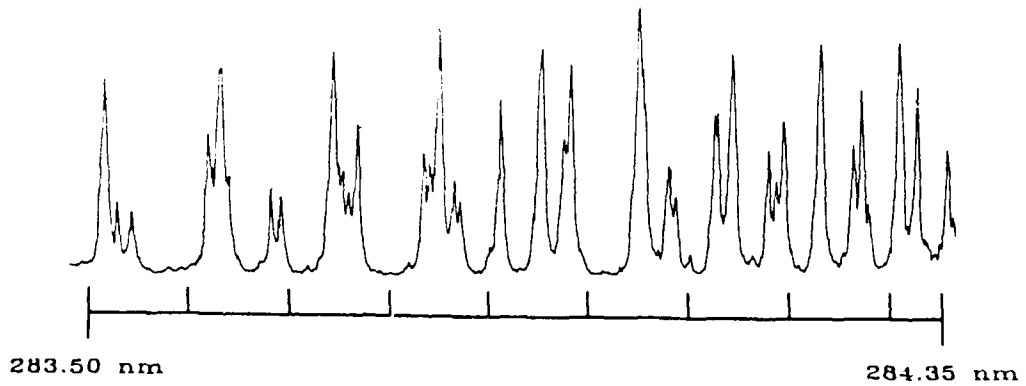
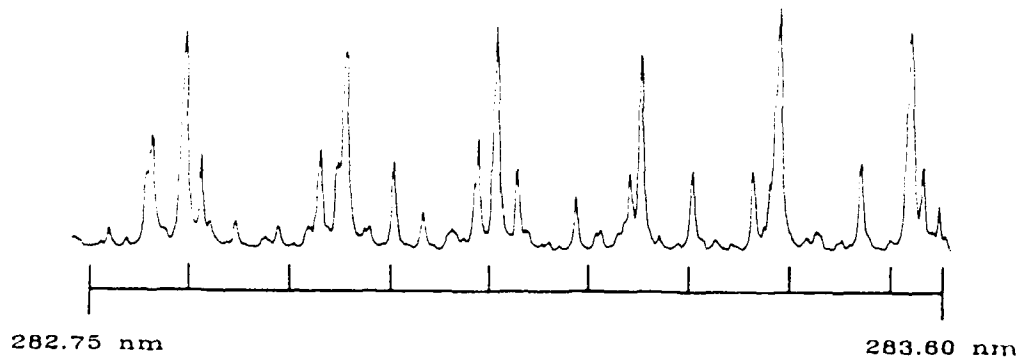
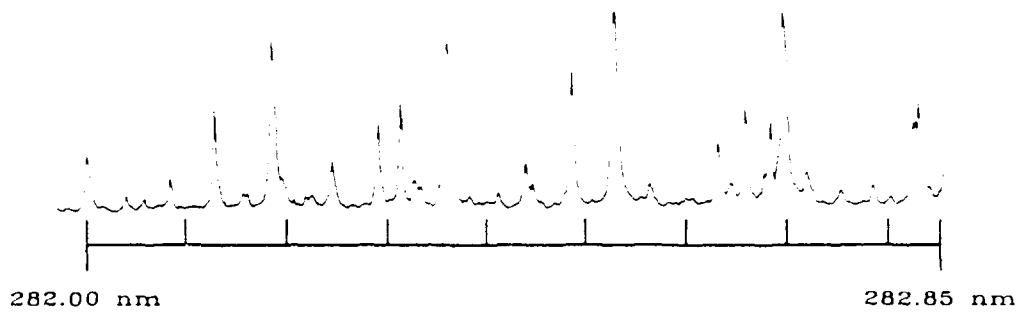
- Figure 1 Schematic diagram of interferometric wavelength reference and calibration system.
- Figure 2 Optogalvanic excitation spectra for portion of nitrogen second positive system between 279.00 and 282.75 nm. Wavelength scales are approximate.
- Figure 3 Optogalvanic excitation spectra for portion of nitrogen second positive system between 282.00 and 285.10 nm. Wavelength scales are approximate.
- Figure 4 Optogalvanic excitation spectra recorded between 280.00 and 280.90 nm. Interferometric calibration signal is also shown. Wavelength scale is approximate.

Table Caption

- Table I Wavelength assignments for selected portion of nitrogen second positive system (see Fig. 4).







Direct Laser Ionization in Analytically-Useful Flames

M.D. SELTZER and R.B. GREEN

Chemistry Division, Research Department
Naval Weapons Center, China Lake, CA 93555

ABSTRACT

Direct laser ionization (DLI) proceeds by resonant excitation of analyte followed by photoionization of the excited state atoms. Photoionization is accomplished using off-resonant radiation which is usually obtained from the dye laser pumping source. DLI has been shown to enhance ionization yields, relative to laser-enhanced ionization (LEI), in low temperature atom reservoirs where collisional ionization is inefficient. In the present study, DLI has been demonstrated in high-temperature, analytically-useful flames with similar results. DLI detection limits, spectral interferences, and the effects of photoionizing laser power on ionization yield have been evaluated.

Index Headings: Direct laser ionization, Laser-enhanced ionization, Photoionization.

INTRODUCTION

Photoionization of excited-state analyte atoms often provides enhancement of ionization yields, relative to single-step laser-enhanced ionization (LEI). This process in a flame was originally referred to as dual laser ionization (DLI) because two lasers were required (1). The name, dual laser ionization, is more historically significant than it is descriptive. The excitation mechanisms by which DLI proceeds are identical to excitation schemes for resonance ionization spectroscopy (RIS) (2) and as such, are not limited to a two laser experiment. The term DLI, meaning direct laser ionization, is retained here to distinguish between resonance ionization in atmospheric pressure atom reservoirs and the typical RIS experiment which is carried out in a low pressure, low temperature atom reservoir such as the source of a mass spectrometer. This usage also preserves the *historical identification*.

DLI and LEI may be viewed as complementary techniques and are similar in their implementation and methodology. In DLI, as in LEI, a dye laser is tuned to a resonant transition of the analyte, resulting in the population of an excited state. LEI proceeds via collisional ionization of analyte atoms from the excited state. In DLI, a second non-resonant laser beam photoionizes the analyte atoms from the bound excited state. The two beams are made spatially and temporally coincident in the atom reservoir. Although collisional ionization always occurs to some extent in most atom reservoirs, the contribution of photoionization to the total ionization signal is greatest when collisional processes alone produce low ionization yields. The photoionizing radiation can, in many cases, be obtained from the same laser that pumps the dye laser, reducing instrumental requirements.

The feasibility of DLI has been demonstrated in both flames (1,3,4) and in plasmas (5,6). Flame temperature determinations based on DLI measurements have also been reported (7). In addition, a DLI approach has been used to enhance ion production in association with diagnostic measurements carried out in an air-acetylene flame (8) and in an inductively-coupled plasma (ICP) (9). Direct laser ionization may provide enhancements of two to three orders-of-magnitude in ionization yield in flames, relative to the LEI approach (4). DLI enhancements of otherwise low ionization yields are maximized when the energy overshoot of the photoionizing laser, into the electronic continuum, is minimized (4). This is best accomplished when the wavelength of the photoionizing laser is well matched to the energy defect between the analyte excited state and the ionization potential. The DLI signal can be increased linearly with increasing power density in the photoionizing beam, and achievement of unity ionization yields is feasible. Therein lies the potential for improving detection limits for atomic transitions which normally have low collisional ionization yields and, hence, poor sensitivity by single-step LEI. The DLI approach also looks appealing because low temperature flames excluding nitrogen may be used more effectively (3). Although collisional ionization yields in similar flames may be low, good DLI detection limits might be obtained without the attendant risk of electrical interferences that occur in hotter flames due to thermal ionization of Group I sample matrix elements. Unfortunately, the lower atom fractions obtained with low temperature flames may offset the benefits of reduced interferences.

The requirements for DLI are similar to those for stepwise or two-color LEI (10,11); the desirability of spatial and temporal coincidence of laser beams is shared by both techniques. Because the latter approach proceeds via two resonant steps, a high degree of spectral selectivity is inherent. DLI, using one resonant step and one

off-resonant step, is inferior in terms of selectivity. The use of off-resonant radiation may result in non-specific, multiphoton ionization (MPI) of background and sample matrix species. Background ionization can contribute significantly to the noise level since its magnitude varies with pulse-to-pulse fluctuations in laser power.

In this paper, the results of a DLI study using air-acetylene and air-hydrogen flames are reported. The atomization efficiency of these flames is superior to flames previously used for DLI (1,3,4,7). Thermal ionization of matrix elements in the hotter flames is correspondingly higher as well. However, the use of a water-cooled, immersed cathode has been shown to permit complete ionization signal recovery in these flames, despite thermal ionization of matrix elements (12). In the present study, DLI experiments were performed using tunable dye laser radiation for the resonant excitation step and the third harmonic (355 nm) of a Nd:YAG pump laser for the off-resonant photoionizing step. The effects of photoionizing laser power, spatial and temporal beam coincidence, and spectral interferences on DLI are discussed. DLI detection limits for strontium and sodium and a comparison of DLI vs. LEI signals in air-acetylene and air-hydrogen flames are also presented.

EXPERIMENTAL SECTION

Figure 1 illustrates the experimental apparatus used for LEI and DLI measurements. A Nd:YAG laser-pumped dye laser (Quantel International, Santa Clara, CA) was operated at a repetition rate of 10 Hz for all experiments. A fraction of the Nd:YAG laser 3rd harmonic (355 nm) was used for the photoionizing beam. Maximum laser pulse energy for photoionization was 20 mJ. The pulsewidth of the laser output was specified by the manufacturer to be 6 to 8 ns. A water-cooled, immersed cathode

and burner head anode were used for signal detection. The applied voltage to the cathode was -1500 V. A preamplifier and boxcar averager (model 162, Princeton Applied Research, Princeton, NJ) provided signal processing. The boxcar aperture duration was 2 ns and the processor module and mainframe time constants were 10 μ s and 1 s, respectively. The boxcar output was recorded with a digital oscilloscope (Model 4094, Nicolet, Madison, WI) or digitized and stored for later processing by a personal computer (model Z-248, Zenith, St. Joseph, MI). All experiments were performed with premixed, partially fuel-lean flames supported on a 1-cm diameter capillary or 5-cm slot burner head. A telescopic beam expander increased the diameter of the resonant excitation beam to 8 mm while maintaining optical saturation. The photoionizing beam was used unfocused, with a diameter of 8 mm.

RESULTS AND DISCUSSION

Strontium and sodium were chosen as test elements for DLI experiments because resonant transitions of these elements coupled well into DLI schemes with small energy overshoots. Figure 2 illustrates the relevant energetics and possible pathways for ionization of strontium and sodium using laser excitation. Shown in Fig. 2 are schemes for LEI, DLI, photoionization of thermally-populated states, and two-photon photoionization of ground-state analyte. Photoionization from thermally-populated states was shown to be negligible in comparison to the other three processes and was not considered further. The DLI schemes illustrated in Fig. 2 involve the same resonant excitation steps as those previously reported (4). In the present work, the 355 nm, 3.5 eV photoionizing beam yields a slightly lower energy overshoot than the shorter wavelength nitrogen laser beam (337.1 nm, 3.68 eV) used

in Ref. 4. The energy overshoot of the 355 nm photoionizing beam is 0.50 eV for strontium and 0.46 eV for sodium.

Laser-Enhanced Ionization. Laser-enhanced ionization measurements were made for strontium and sodium in both the air-acetylene and air-hydrogen flames according to the excitation scheme shown in Fig. 2a. The LEI measurements were made by blocking the photoionizing beam and illuminating the flame with resonant radiation only. It was determined that the excitation step for both elements was optically saturated by attenuating the resonant laser beam with calibrated filters and observing the corresponding LEI signal. The resulting plot of ionization signal vs. laser power revealed a distinctive plateau region that is characteristic of optical saturation of the excitation step. LEI detection limits for strontium and sodium in the respective flames are given in Table I.

Two-Photon Ionization. In the absence of resonant excitation, ionization signals were observed for strontium and sodium due to illumination with the 355 nm photoionizing beam. Simultaneous absorption of two photons from the photoionizing beam at 355 nm can proceed, through a virtual level, to ionize ground state analyte atoms. Figure 3 is a plot of strontium ionization signal vs. percent laser power using the 355 nm beam only. This data indicates that the ionization signal varies as the square of the laser power, suggesting that a two-photon interaction (Fig. 2d) predominates over thermally-assisted photoionization (Fig. 2c). When both resonant radiation and UV photoionizing radiation are used (Fig. 2b), as in DLI, resonant excitation competes with the two-photon process for ground state analyte atoms. The resonant pathway to ionization is preferable for analytical work, because of its inherent spectral selectivity. The probability of absorption of an off-resonant photon is much lower than that for resonant absorption. However, the lower

probability for two-photon absorption may be offset by the high power in the photoionizing beam.

Effect of Photoionizing Beam Power on DLI Signals. Optical saturation of the DLI resonant excitation step was confirmed for both strontium and sodium. The photoionizing step itself is not optically saturable in the traditional sense, since it does not involve a resonant transition. In addition, the ionization continuum acts as a trap for excited atoms preventing re-population of the bound excited state. Figure 4 is a plot of DLI signal vs. percent incident laser power at 355 nm. This plot was obtained by making DLI measurements for a 10 $\mu\text{g/mL}$ solution of strontium while optically saturating the excitation step (460.7 nm) and incrementally adjusting the power of the photoionizing beam. Blank measurements were subtracted at each power level. The signal vs. power plot shows mostly linear character which suggests that the DLI mechanism, resonant excitation followed by photoionization (Fig. 2b), is the predominant pathway to ion production under these conditions. However, at the highest power levels some nonlinearity indicates a possible two-photon ionization contribution to the total signal. It may not be possible to separate the contribution of two-photon ionization from the total signal, but this study of DLI signal vs. photoionizing beam power confirms its existence.

Temporal Coincidence of Resonant and Photoionizing Laser Beams. Stepwise laser excitation requires that photons of the overlapped beams are temporally coincident at their intersection in the flame. The second-step photon may be delayed slightly, depending on the lifetime of the excited state populated by the first photon (13). Laser radiation used in the DLI experiments reported here is derived from both pump and dye laser outputs. Consequently, radiation from the two lasers may not be temporally coincident at the intersection of the two beams. For

lasers with ns pulsewidths, the temporal coincidence of the two beams in the flame can be conveniently manipulated by adjusting the optical path length of one beam with respect to the other. In the work reported here, the arrival of the UV photons was delayed optically as shown in Fig. 1. By adjusting the optical delay of the photoionizing beam and observing the magnitude of the DLI signal, the existence of an optimum delay was established. However, DLI signals obtained at optimum delay of the photoionizing beam were only twice as large as those obtained at non-optimum delays. This suggests that significant temporal overlap exists between the two laser beams with respect to coupling of the excitation step to the photoionization step for the configuration used. In fact, the largest DLI signals by far were obtained when the delay line was eliminated and transmission power losses in the photoionizing beam were minimized.

Spatial Coincidence of Resonant and Photoionizing Laser Beams. In DLI or any multistep excitation scheme, only the volume of analyte atoms intersected by all radiation sources will experience the effects of the combined interaction of the various beams. Since it may be advantageous to optimize the diameter of the resonant excitation beam under optical saturation conditions, it becomes necessary to match the beam diameter of the photoionizing beam to that of the resonant beam. This is important because any photoionizing radiation that does not coincide with resonant radiation will not contribute to the DLI signal but will induce additional background ionization. In the present study, the two 8-mm diameter laser beams intersected in the flame at an angle of approximately 20 degrees. This arrangement facilitated the maximum overlap of the two beams. The positions of the two beams were carefully adjusted while the DLI signal for strontium was monitored.

During the process of aligning the two laser beams in the flame, an ionization signal was observed for strontium and sodium, respectively, even when there was no overlap between the two beams. The total ionization signal produced by the two non-coincident beams was significantly larger than the sum of the ionization signals recorded separately for 460.7 nm (or 589 nm) and 355 nm excitation. This unaccounted for signal was observed when the two beams were vertically displaced from each other in the flame by as much as 3 cm, and occurred regardless of which beam was positioned nearest the cathode.

It was experimentally confirmed that the total ionization current should equal the sum of separately-generated ionization signals by splitting the 355 nm beam equally and directing the separated beams into a flame. The total ionization signal recorded for irradiation with both 355 nm beams simultaneously was equal to the sum of the ionization signals recorded separately for the two beams. A similar experiment, splitting the 460.7 nm beam, resulted in an identical result although this produced LEI rather than photoionization signals.

Although the unaccounted for signal was first observed with a capillary burner head and an air-acetylene flame, further investigations were conducted with the slot burner head with an air-hydrogen flame to eliminate the signal dependence on differences in atom fractions and collecting fields at different heights in the flame and to reduce the possibility of electrical interferences. The two laser beams were separated laterally by 2 cm and positioned at the same height in the flame near the surface of the same water-cooled electrode, aligned along the length of the slot. Fig. 5a illustrates the illumination geometry of the slot burner-supported flame. The results for an experiment recording strontium ionization signals for the non-coincident beams, alternately blocking one of the beams and illuminating the flame

with both beams are shown in Fig. 5b. The total ionization signal obtained when both beams were used is greater than the sum of the signals arising from illumination by individual beams.

Reversing the position of the beams in the capillary burner eliminated the possibility that atoms excited by 460.7 nm radiation were being ionized by the 355 nm beam higher in the flame. Observation of the unaccounted for signal with a 460.7 and a 355 nm beam in the side-by-side configuration corroborated this finding.

The possibility that strontium resonance atomic fluorescence, excited by 460.7 nm radiation, was responsible for exciting strontium atoms residing in the 355 nm beam volume was also considered. The excited strontium atoms would then be photoionized. A ceramic plate was inserted into the air-hydrogen flame to act as a barrier to create two regions of the flame which were separately illuminated by the 460.7 and 355 nm beams. The ceramic plate blocked any resonance fluorescence traversing the flame and did not appear to perturb the flame greatly. Ionization signals were recorded for illumination by the individual beams and for simultaneous illumination by both beams. The total signal recorded for simultaneous illumination by both beams was again greater than the sum of the individual signals. The total signal was, however, smaller than that observed without the ceramic plate in the flame. These results suggested that since fluorescence was effectively eliminated as an optical pathway for energy transfer within the flame, it was not responsible for the anomalous signals resulting from excitation by non-coincident beams. At present, the origin of the anomalous signals is not understood. We are currently planning experiments to further study this phenomenon.

Spectral Interferences. The use of a UV laser beam to enhance analyte ionization yields carries with it the risk of non-specific, multiphoton ionization of background and matrix species. Similar interferences have been observed in the present study and are most serious at high laser powers as indicated by the second-order power dependence of the signals. Two-photon photoionization by the 355 nm beam was observed for calcium, lithium, and sodium as well as strontium. The relative signal strengths for these easily-ionized elements and the interference effects of calcium on measurements of strontium ionization signals in the air-hydrogen flame are summarized in Tables II and III. Additional signal from photoionization of calcium caused a significant positive interference for DLI of strontium. Multiphoton-induced ionization of both water and flame species was also observed for both the air-acetylene and air-hydrogen flames.

Since the optimum region of the flame for illumination is adjacent to the immersed cathode where the collecting field is strongest, it is advantageous to position both beams as close to the cathode as possible. When a UV photoionizing laser is used, photoelectric emission due to inadvertent illumination of the metal cathode may be a source of noise but it can be minimized by careful alignment.

Detection Limits. Detection limits for DLI measurements were extrapolated from calibration curves with slopes of one and defined as the concentration of analyte which would produce a signal equal to three times the standard deviation of the blank signal. The detection limits obtained by DLI for the test elements, strontium and sodium, are listed in Table I for both air-acetylene and air-hydrogen flames, along with the corresponding LEI detection limits which were calculated in the same manner. Also shown are the DLI enhancements of the ionization yield, which represent the DLI to LEI signal ratios. The DLI detection limits in Table I are

measurements made with maximum photoionizing laser power, which produced the largest enhancement of the ionization signal. The LEI and DLI detection limits reported here were obtained with 10 Hz laser repetition rate in flames supported on a 1-cm diameter capillary burner. Consequently, these detection limits are inferior to LEI detection limits reported in the literature obtained with higher repetition rate lasers in flames supported on longer path length slot burners. The capillary burner was used in the present case to facilitate maximum overlap of the two laser beams in the flame.

The largest DLI enhancements (Table I) were observed for strontium, in both the air-acetylene and air-hydrogen flames. In the air-acetylene flame, higher temperatures (ca. 2450 K) result in higher rates of collisional ionization for strontium than in the cooler (ca. 2300 K) air-hydrogen flame. Therefore, collisional ionization in the air-acetylene flame makes a greater contribution to the total signal under DLI conditions, leading to a lower DLI enhancement. Collisional ionization of the strontium 5p level is far from complete in either flame as evidenced by the strontium LEI detection limits. This is due to the large 3.00 eV energy defect between the strontium 5p level and the 5.69 eV ionization potential. Collisional ionization from the sodium 3p level was equally limited due to the 3.04 eV energy defect between this level and the 5.14 eV ionization potential of sodium. However, only a factor of two DLI enhancement for sodium was observed in either flame.

The DLI improvements in detection limit in the present study for strontium, relative to LEI, are less than one might expect considering the relative increase in ionization yield afforded by DLI. However, increases in the background noise due to the addition of a high-power photoionizing beam negate, to some extent, the advantage of increased ionization yield. Also, since the magnitude of the DLI

enhancement is highly dependent on laser power, the enhancements obtained may not be reproducible on a day-to-day basis, and may require normalization to compensate for long-term drift in laser output.

CONCLUSIONS

The feasibility of DLI in analytically-useful flames has been demonstrated. Although the flames used here generally provide adequate collisional ionization for LEI, the use of atomic transitions that exhibit large energy defects lowers ionization yields. The addition of a high-power photoionizing beam with a minimum energy overshoot allowed large enhancement of ionization yields for strontium, relative to LEI excitation. Detection limits obtained with DLI for strontium were superior to LEI detection limits obtained with the same instrumentation. The DLI detection limits reported here and elsewhere, are inferior to those reported in the literature for two-step LEI. DLI enhancement of sodium ionization yields in either flame was less than anticipated. A DLI enhancement of 100 was previously reported for sodium in a hydrogen-oxygen-argon flame (4). It is likely that collisional ionization yields for sodium were extremely low in that relatively cool (ca. 1800 K), nitrogen-excluding flame thus allowing considerable DLI enhancement. In the air-hydrogen and air-acetylene flames used in the present study, collisional ionization of the sodium 3p level was undoubtedly more efficient, yet incomplete. Similar DLI enhancement of sodium ionization in both flames suggests that collisional ionization of excited state sodium atoms in both flames proceeds to a similar degree. The large difference between DLI enhancements of strontium and sodium obtained under similar conditions (optically saturated excitation step, large energy defect, similar photoionizing energy overshoot) may be attributed in part to differences in the

collisional ionization kinetics of the two elements as well as differences in photoionization cross-section. It has been suggested that autoionizing levels may also play a decisive role in determining photoionization yields (8). Autoionizing levels may be most dense just above the ionization limit, hence, the advantage in minimizing photoionizing energy overshoot. However, the greatest enhancement of ionization yield occurs when resonance is achieved with an autoionizing level. This may have been the case with strontium in the present study. Autoionization may have been responsible for the large sodium DLI enhancement reported in Ref. 4 as well.

Further optimization of burner and illumination geometry may result in higher sensitivity for DLI. Increasing the power density of the photoionizing beam could produce larger DLI enhancements, but will likely result in larger background signals. Although background signals can be accounted for by a simple blank subtraction or by scanning the excitation laser off-line, the noise contribution from these background signals remain, and degrade DLI sensitivity.

The performance of DLI also may be improved by optimizing the wavelength of the photoionizing laser to reduce the energy overshoot to zero, thereby increasing the photoionization yield. However, when two tunable dye lasers are available, it is preferable to perform two-step selective excitation of the analyte to high-lying atomic levels where the ionization yield approaches unity. The benefits of high sensitivity and the improved selectivity of two-step LEI outweigh the simplicity advantage and the potential for increased signal using the DLI approach.

ACKNOWLEDGMENT

Michael D. Seltzer was supported on an Office of Naval Technology Postdoctoral Fellowship which is administered by the American Society for Engineering Education.

References

1. C. A. van Dijk, F. M. Curran, K. C. Lin, and S. R. Crouch, *Anal. Chem.* **53**, 1275 (1981).
2. G. S. Hurst, M. G. Payne, S. D. Kramer, and J. P. Young, *Rev. Mod. Phys.* **51**, 767 (1979).
3. F. M. Curran, C. A. van Dijk, and S. R. Crouch, *Appl. Spectrosc.* **37**, 385 (1983).
4. F. M. Curran, K. C. Lin, G. E. Leroi, P. M. Hunt, and S. R. Crouch, *Anal. Chem.* **55**, 2382 (1983).
5. M. E. Churchwell, T. Beeler, J. D. Messman, and R. B. Green, *Spectrosc. Lett.* **18**, 679 (1985).
6. M. D. Seltzer and R. B. Green, *Spectrosc. Lett.* **20**, 601 (1987).
7. K. C. Lin, P. M. Hunt, and S. R. Crouch, *Chem. Phys. Lett.* **90**, 111 (1982).
8. G. C. Turk and N. Omenetto, *Appl. Spectrosc.* **40**, 1085 (1986).
9. G. C. Turk, O. Axner, and N. Omenetto, *Spectrochim. Acta* **42B**, 873 (1987).
10. G. C. Turk, J. R. Devoe, and J. C. Travis, *Anal. Chem.* **54**, 643 (1982).
11. I. Magnusson, O. Axner, and H. Rubenzstein-Dunlop, *Phys. Scripta* **33**, 429 (1985).
12. G. C. Turk, *Anal. Chem.* **53**, 1187 (1981).
13. N. Omenetto, T. Berthoud, P. Cavalli, and G. Rossi, *Appl. Spectrosc.* **39**, 500 (1985).

Table I. Detection Limits for Laser-Induced Ionization of Strontium and Sodium.

Flame	Element	Detection Limits (ng/mL)		DLI Signal Enhancement
		LEI	DLI	
air-hydrogen	Sr	3	0.03	134
	Na	0.8	0.5	2
air-acetylene	Sr	1	0.02	78
	Na	0.6	0.3	2

Table II. Comparison of Ionization Signals for 355 nm Excitation in an Air-Hydrogen Flame.

Element	Concentration	Relative Signal
Sr	10 $\mu\text{g/mL}$	8.4
Ca	10 "	7.3
Li	10 "	1.7
Na	10 "	1.0

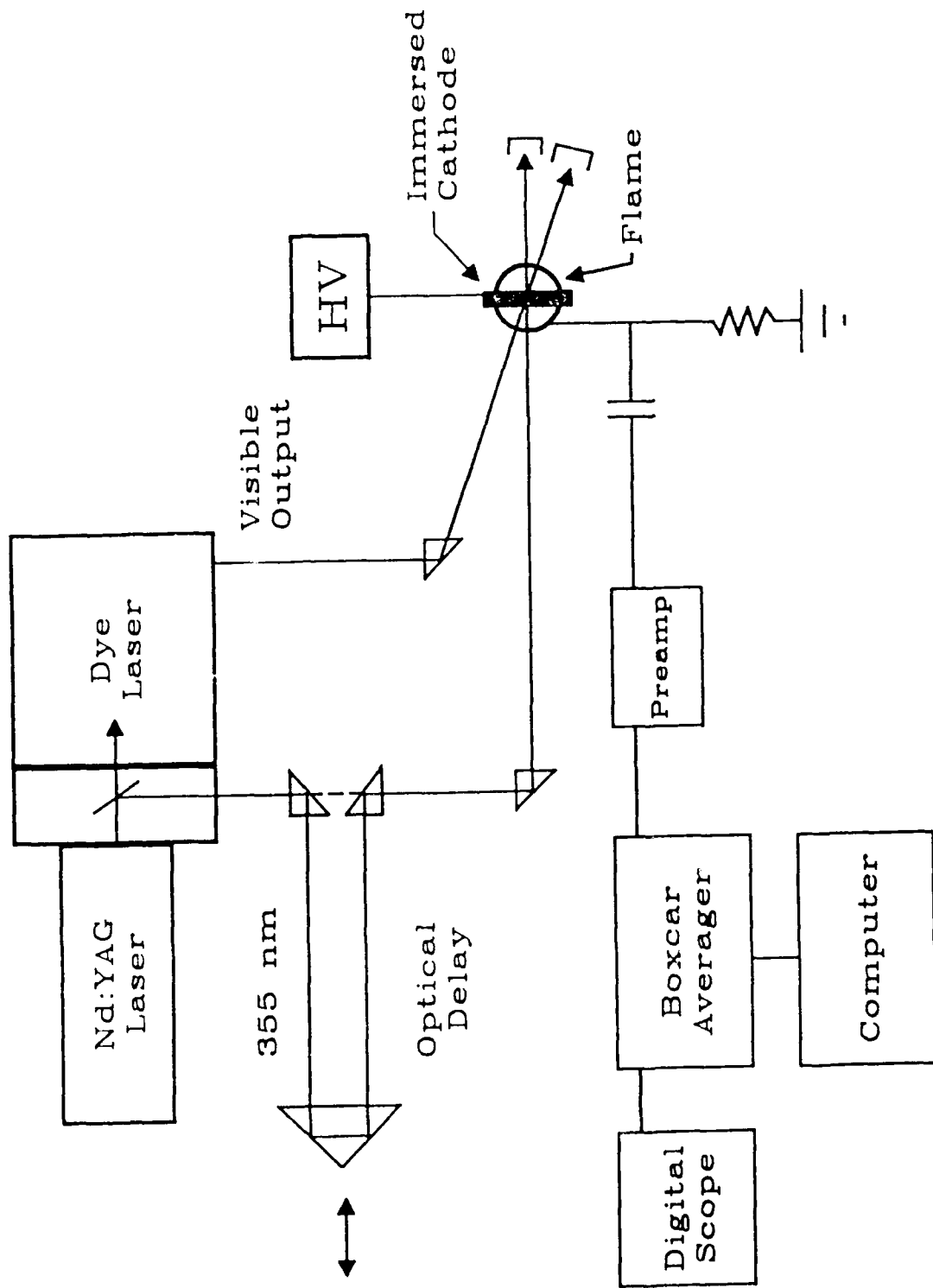
Table III. Calcium Ionization Interferences with LEI and DLI of Strontium in an Air-Hydrogen Flame.

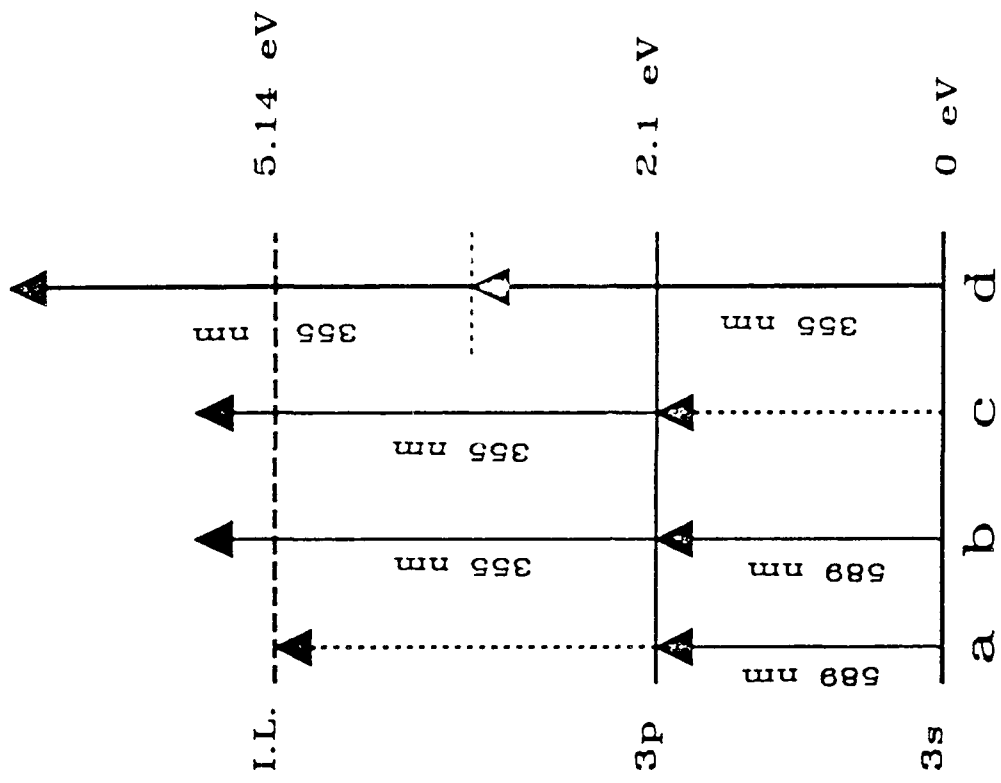
<u>LEI</u>	<u>Signal</u>
Sr, 500 ng/mL	0.15
Sr, 500 ng/mL, Ca 5 μ g/mL	0.16

<u>DLI</u>	<u>Signal</u>
Sr, 500 ng/mL	25
Sr, 500 ng/mL, Ca, 5 μ g/mL	39

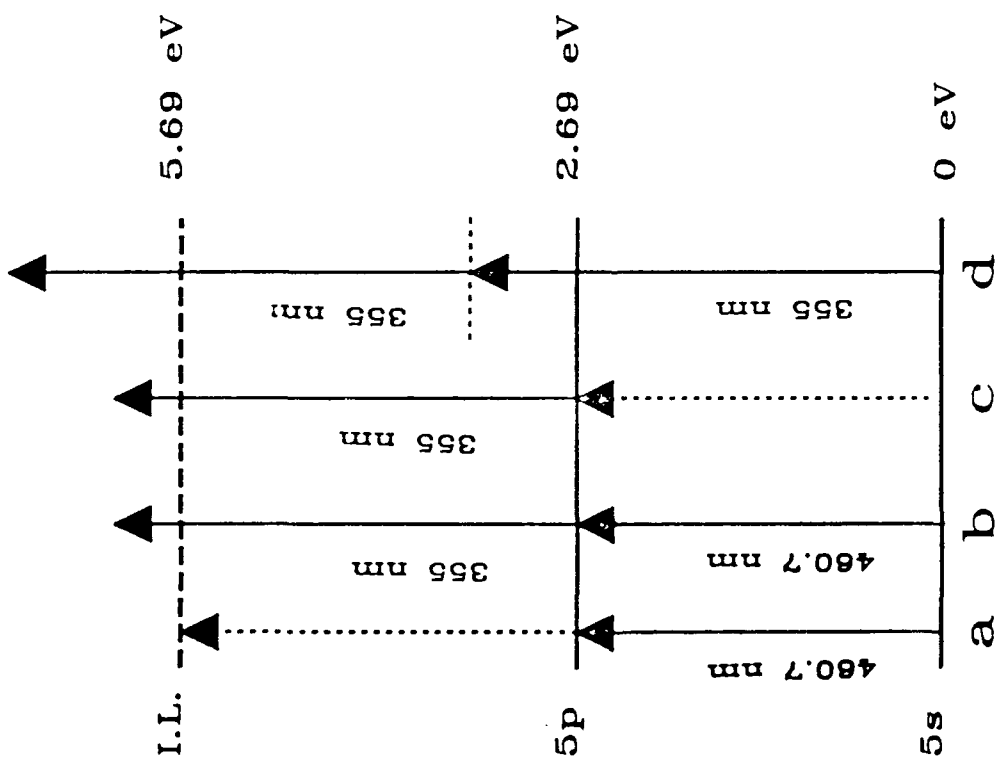
Figure Captions

- Fig. 1. Schematic diagram of DLI instrumentation. Telescopic beam expander has been omitted.
- Fig. 2. Energy level diagram for excitation and ionization of strontium and sodium. a) LEI; b) DLI; c) Thermally-assisted photoionization; and d) Two-photon photoionization of ground-state analyte.
- Fig. 3. Effect of photoionizing laser power on strontium ionization signal.
- Fig. 4. Effect of photoionizing laser power on strontium DLI signal.
- Fig. 5. (a) Illumination geometry of slot burner-supported flame, (b) ionization signals for 40 ng/mL strontium in an air-hydrogen flame using configuration (a).





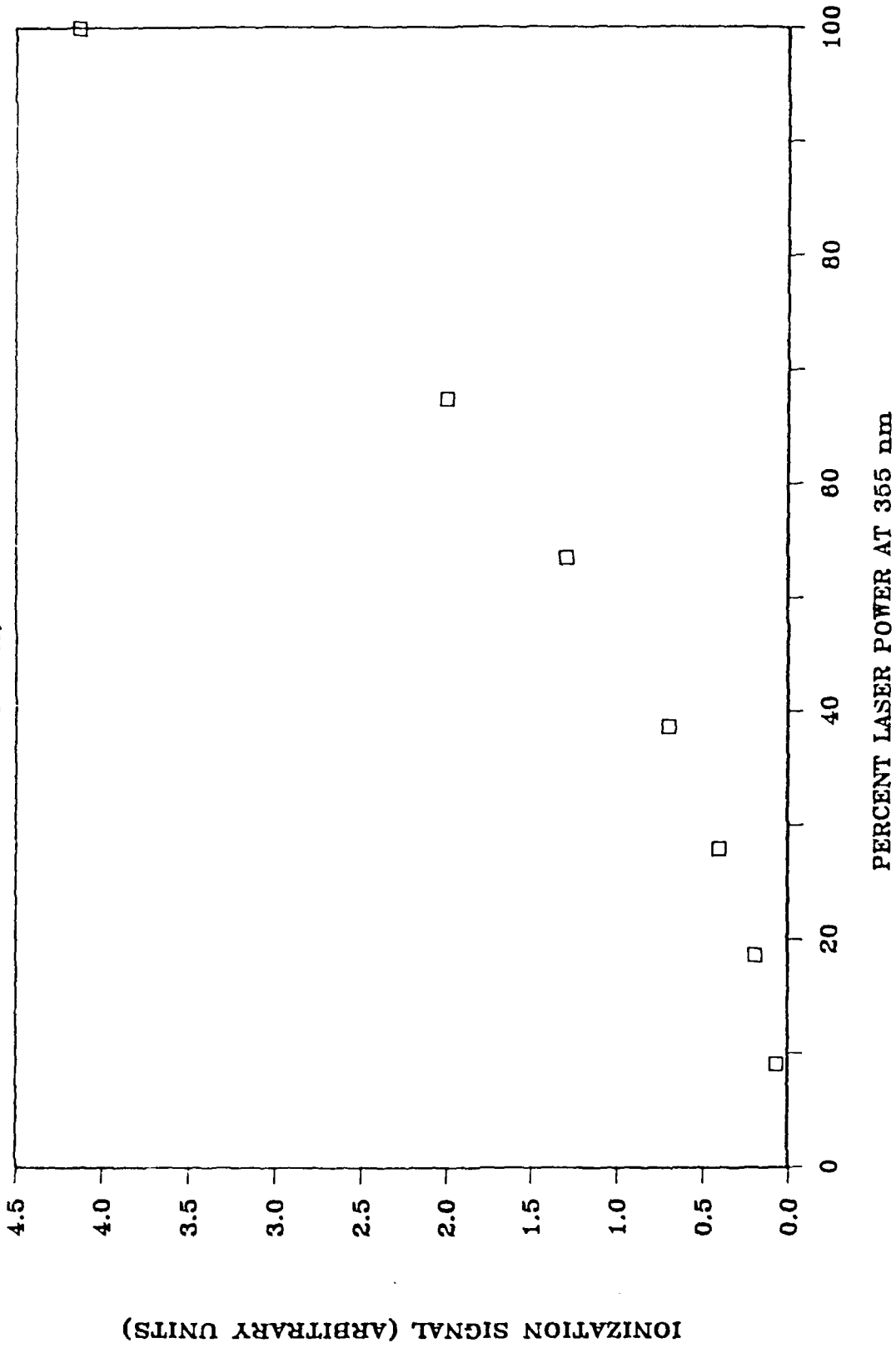
Na



Sr

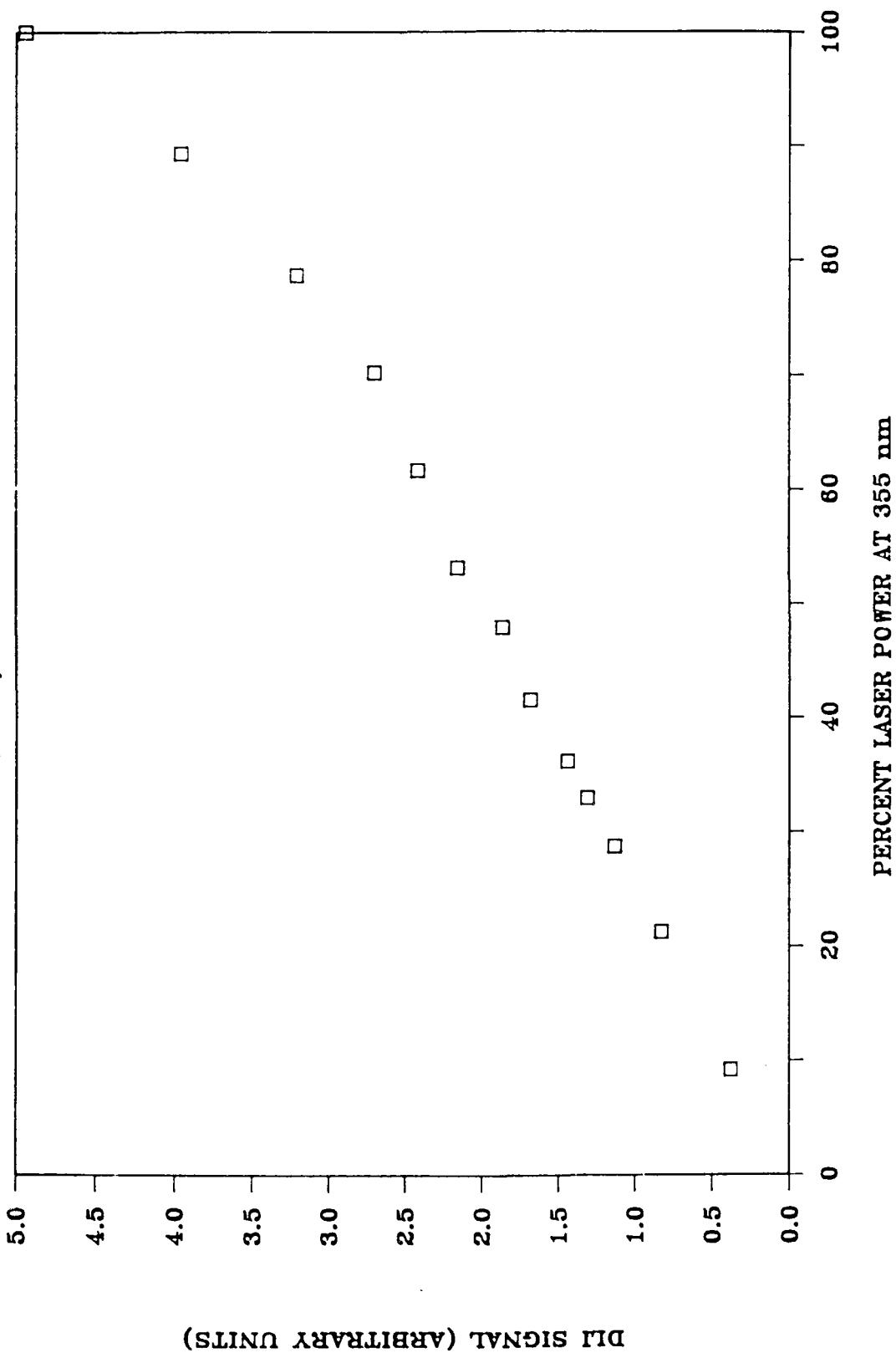
IONIZATION SIGNAL VS. LASER POWER

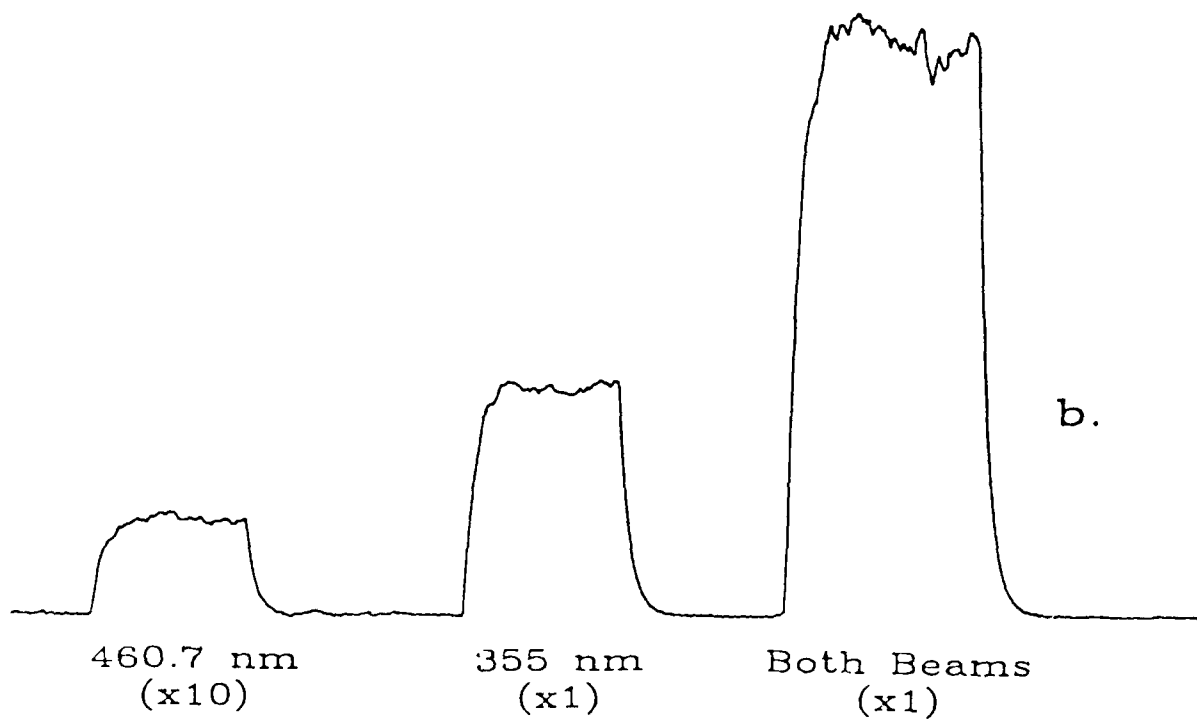
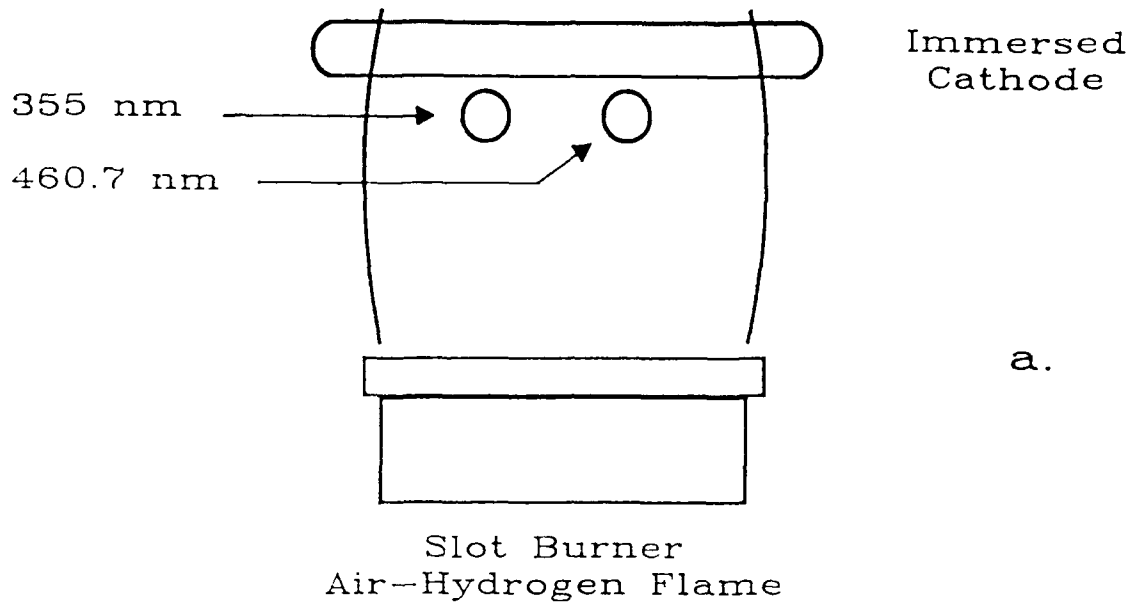
STRONTIUM, 355 nm



DLI SIGNAL VS. LASER POWER

STRONTIUM, 460.7/355 nm





LASER POWER DEPENDENCY OF RESONANCE IONIZATION IN FLAMES

M.D. Seltzer and R.B. Green

Chemistry Division, Research Department

Naval Weapons Center, China Lake, CA 93555

ABSTRACT

Resonant two-photon ionization competes with laser-enhanced collisional ionization (LEI) in flames to ionize analyte atoms. The predominance of either mechanism for a given element depends on the excitation scheme as well as the level of irradiance. Optical saturation of the resonant transition through which the two-photon mechanism proceeds precludes observation of a second order dependence of ionization signal on laser power. The laser power dependency of resonant two-photon ionization for a series of elements is examined and results of diagnostic value regarding the probable ionization mechanisms are obtained.

Index Headings: Resonance ionization, Laser-enhanced ionization, Photoionization.

LASER POWER DEPENDENCY OF RESONANCE IONIZATION IN FLAMES

INTRODUCTION

This paper examines the dependence of resonance ionization in flames on incident laser power. The basis for resonance ionization spectroscopy (RIS) (1) is the absorption of two or more photons with at least one in resonance, providing sufficient energy to directly ionize analyte atoms. In the simplest case, this can be accomplished using two photons of equal wavelength from a single laser source, given that the photon energy exceeds one-half the value of the atom's ionization potential. Proportional counters or pulsed ionization chambers are generally used as detectors in RIS. RIS techniques involve direct photoionization, rather than collisional ionization processes because the latter are relatively infrequent in the low temperature, low pressure environment in which RIS is carried out. In RIS techniques, highly focussed laser beams are typically used to produce the large power densities required to saturate the ionization process. Resonant two-photon ionization mechanisms have been demonstrated for approximately fifty elements using a single laser for resonance ionization mass spectrometry (RIMS) (2). Resonance ionization schemes have been carried out in flame atom reservoirs as well, but have been more commonly referred to as direct or dual laser ionization (DLI) (3,4).

In flames, collisional ionization of analyte atoms always occurs to some extent whether or not laser excitation is present. In laser-enhanced ionization (LEI) in flames and in other atom reservoirs (5), resonant photons from one or two lasers are used to enhance the rate of collisional ionization of analyte atoms. LEI and DLI are

complementary techniques and are detected by measuring the electrical impedance changes that occur in response to the laser-induced formation of ion-electron pairs in the atom reservoir. In LEI, the rate of collisional ionization is greatest when the energy defect (Figure 1), or difference in energy between the laser-populated excited state and the ionization limit, is minimized. When a large energy defect exists between the laser-populated excited state and the ionization potential, the probability of collisional ionization, following the absorption of a single photon, may be extremely low and absorption of a second identical photon to directly photoionize analyte atoms (i.e., DLI) may compete with collisional processes to ionize analyte atoms. At the relatively low levels of spectral irradiance commonly used for LEI spectrometry, the collisional pathway is often more probable due to the low photoionization cross-section for excited state atoms. At higher levels of irradiance, the low probability for absorption of a second photon may be offset by the increased irradiance and the resonant two-photon mechanism may predominate (6). The result will often be a substantial increase in ionization yield.

The probability or cross-section for resonant two-photon ionization is determined in part by the degree of energy overshoot (Fig. 1) of the second photon into the ionization continuum (7). Resonant two-photon ionization schemes with small energy overshoots are more favorable and should contribute significantly to the total ionization signal even at low levels of irradiance. Autoionizing levels may also play an important role (8,9)

Many resonant atomic transitions can be optically saturated with moderate laser power (10). When the resonant transition is optically saturated, the absorption coefficient for that transition approaches zero and there is no net increase in the population of the upper level due to additional incident photons. Consequently, there

is no net increase in the rate of laser-induced collisional ionization with increasing irradiance. The onset of optical saturation is typified by less than linear power dependence of the ionization signal. Beyond the saturation threshold, the slope of the ionization signal vs. irradiance plot rapidly approaches zero.

Resonant two-photon ionization generally requires levels of laser irradiance that exceed the saturation thresholds of the resonant transitions through which it proceeds. Therefore, resonant two-photon ionization in flames may not be apparent until after the first resonant absorption transition is far into optical saturation. Two-photon mechanisms are characterized by slopes of two on log-log plots of ionization signal vs. laser power due to the second order power dependence of the signal. However, when those mechanisms proceed through resonant transitions that are optically saturated, the rate of excitation by the first resonant photon is independent of laser irradiance and absorption of the second photon becomes the rate-limiting step (2). Consequently, second order power dependence is not observed, despite the existence of a two-photon pathway to ionization. Subsequent increases in laser power may result in only linear increases in ionization yield.

Optical saturation does not occur for some resonant transitions at the low levels of laser irradiance commonly used in analytical work. However, optical saturation is not a prerequisite for resonant two-photon ionization. It is possible, therefore, that resonant two-photon ionization for some elements in flames will be evident at levels of irradiance that are lower than those required to optically saturate the resonant transition. If the resonant transition is not optically saturated, ionization should increase linearly with laser power as long as first-order laser-induced collisional ionization is predominant. At sufficiently high laser power, the rate of resonant two-photon ionization overtakes that of the competing collisional

mechanism. In the absence of optical saturation of the resonant step, a second-order power dependence should then be evident for the two-photon process. Over this range, a log-log plot of ionization signal vs. laser power should yield a slope of two.

Resonant two-photon ionization in flames allows increased ionization yields relative to one-step LEI excitation but generally requires higher laser power levels than those typically used for conventional flame LEI. The predominance of either of two competing mechanisms for ionization depends strongly on factors that directly influence the relative probability of those processes for given atomic transitions. The present paper illustrates several examples of the relationship between resonant two-photon ionization, laser-induced collisional ionization, laser power, and the ability to optically saturate the resonant transition. The effects of energy defect and energy overshoot in determining the dominant pathway to ionization are emphasized.

EXPERIMENTAL SECTION

The instrumentation used for the present study is similar to that described in ref. 4. A Nd:YAG laser-pumped dye laser (Quantel International, Santa Clara, CA) with frequency doubling and mixing capability was operated at a repetition rate of 10 Hz. Rhodamine 590 and a mixture of rhodamine 590 and rhodamine 610 laser dyes (Exciton, Dayton, OH) were used to generate fundamental radiation over a wavelength range of 550 to 595 nm. The fundamental output was either used unaltered, frequency doubled, or mixed with the Nd:YAG fundamental (1064 nm) to generate the excitation wavelengths. The laser pulsewidth and spectral bandwidth were specified by the manufacturer to be 6-8 ns and 0.003 nm, respectively. Incident laser power

was controlled using two variable laser attenuators (model 935-5, Newport, Fountain Valley, CA) in series. Laser power was monitored by illuminating a fast photodiode with a fraction of the laser beam and observing the output of the photodiode with an oscilloscope. A 1-cm diameter capillary burner supported an air-hydrogen flame in all experiments. A 300 mm focal length lens was used to partially focus the laser beam in the flame to an approximate spot size of 1 mm. This arrangement was chosen to insure homogeneous irradiance of the flame through the entire volume intersected by the laser beam. Tighter focussing of the laser beam results in localized effects which may not reflect the true laser power dependency (11). Ionization was detected using a water-cooled, immersed cathode, biased at -1500 V, and the burner head as the anode. Signals collected at the anode were preamplified and fed to a boxcar averager (model 162, Princeton Applied Research, Princeton, NJ). The boxcar aperture duration and integrator time constant were 2 and 10 μ s, respectively. The boxcar output was displayed on a digital oscilloscope (model 4094, Nicolet, Madison, WI), digitized and stored on a personal computer (model Z-248, Zenith, St. Joseph, MI) for processing and display.

RESULTS AND DISCUSSION

For the series of test elements used in the present work, sample solutions of 1 to 10 μ g/mL were aspirated into the air-hydrogen flame. The air-hydrogen flame was chosen as an alternative to the air-acetylene flame which generates considerable background due to multiphoton ionization of hydrocarbon species. The wavelength of the dye laser was optimized prior to each experiment by tuning the unfocussed laser beam to a particular atomic transition using the lowest possible

irradiance to avoid saturation broadening and subsequent distortion of the line profile (12). Transitions were selected for the various test elements that satisfied the requirements for resonant two-photon ionization, i.e., the combined energy of two photons must be sufficient to excite the atom into the ionization continuum. The energy diagram in Figure 1 illustrates this point. The test elements, resonant transitions, transition probabilities, relevant energy levels, energy defects, and energy overshoots, are listed in Table I. To investigate the laser power dependency of resonant two-photon ionization for each element, incident laser power was incrementally adjusted, and the ionization signal and relative power value were recorded. Blank signals were also recorded at each power increment. Ionization signals were sampled for 10 seconds (100 laser pulses). For each of the elements and transitions investigated, log-log plots of net ionization signal vs. laser power were constructed. Figures 2 through 7 illustrate the laser power dependency of the ionization signals recorded for the test elements listed in Table I. Laser power values on each log-log plot are relative. The levels of irradiance used in the various experiments were similar, up to 120 MW/cm^2 and the power values have been normalized to the same log scale. Each ionization signal plotted in Figures 2-7 represents the average of 100 measurements with an approximately 5% R.S.D.

Strontium. The strontium transition at 293.2 nm is not easily saturated at moderate laser powers as suggested by its low transition probability (Table I). The energy defect of $11,828 \text{ cm}^{-1}$ is reasonably low to allow for adequate collisional ionization from the laser-populated level at $34,098 \text{ cm}^{-1}$. Figure 7 shows that the strontium ionization signal increases linearly (with a slope of one) up to a distinctive break point where the slope changes abruptly to a value of two. This point represents the laser power at which the rate of two-photon ionization overtakes that of single-photon enhanced, collisional ionization. No optical saturation of the strontium

resonant transition at 293.2 nm was evident and therefore, second-order power dependence was preserved. Although the two-photon energy overshoot for this transition is large, at sufficient laser power, the two-photon mechanism predominates as indicated by the second order power dependence beyond the break point.

Sodium. The sodium transition at 589.0 nm originates $16,973 \text{ cm}^{-1}$ above the ground state. The transition is easily saturated and has a small energy defect of $6,901 \text{ cm}^{-1}$. Two-photon ionization of sodium using the 3p-4d resonant transition is a special case because the photon energy is less than one-half the ionization potential. However, because the process originates at a level that is $16,973 \text{ cm}^{-1}$ above the ground state, two-photon ionization is still possible. Two-photon absorption from an excited state may be generally less probable than from the ground state. However, this penalty is compensated for by the moderate energy overshoot of $10,675 \text{ cm}^{-1}$. Figure 6 illustrates power dependence of the ionization signal when sodium is excited at 589.0 nm. It is assumed, based on the log-log plot, that there was no net increase in the rate of laser-induced collisional ionization beyond the level of irradiance required to optically saturate the excited state resonant transition of sodium. After a brief saturation plateau, the ionization signal was observed to increase linearly (slope of one) with laser power. The post-saturation increase in ionization signal with laser power was most probably due to the absorption of a second resonant photon although the expected second-order power dependence was obscured by optical saturation of the first resonant step.

Gallium. The gallium transition at 294.4 nm, is easily saturated as a consequence of its large transition probability (Table I). The small energy defect of $13,593 \text{ cm}^{-1}$ makes this transition favorable for LEI work. For two-photon ionization at 294.4 nm,

there is a considerable energy overshoot of $20,368 \text{ cm}^{-1}$. Figure 2 is a log-log plot of LEI signal vs. laser power for gallium. In Figure 2, the signal is observed to increase linearly with laser power up to the point of optical saturation, at which a plateau is evident. After a further increase in laser power, the signal again increases linearly (slope of one) with laser power. Although the two-photon pathway to ionization becomes predominant after the resonant transition leading to collisional ionization has been optically saturated, a second-order power dependence is not observed. This behavior is analogous to that observed for the optically saturated sodium transition.

Thallium. The thallium transition at 377.6 nm was excited with radiation obtained by frequency-mixing the dye laser fundamental with a fraction of the Nd:YAG fundamental. This transition is easily saturated but has a moderately large energy defect of $22,786 \text{ cm}^{-1}$. The energy overshoot for two-photon ionization, of $3,692 \text{ cm}^{-1}$ is the smallest encountered in the present study. Figure 4 illustrates the laser power dependency for ionization of thallium, excited at 377.6 nm . The signal increases linearly until a brief saturation plateau is reached. The signal then almost immediately begins to increase linearly with laser power. Because of the large energy defect, collisional ionization may not be very efficient. The small energy overshoot increased the probability for two-photon ionization, hence its appearance soon after the saturation point of the resonance transition.

Cobalt. The cobalt transition at 292.9 nm is relatively weak (Table I) suggesting that considerably high irradiance might be needed to optically saturate the transition. The large energy defect (Figure 3) of $29,304 \text{ cm}^{-1}$ is not conducive to efficient collisional ionization, and therefore, this transition is not optimum for conventional LEI use. However, a two-photon ionization scheme using the same resonant transition results in a small overshoot of $4,830 \text{ cm}^{-1}$. The log-log plot of ionization

signal vs. laser power in Figure 3 shows a slope of two at low laser power with some deviation (slope less than two) at higher power. This suggests that collisional ionization following one-photon excitation was not appreciable due to the large energy defect and, therefore, the two-photon mechanism was predominant even at low laser power. The slope deviation observed at higher powers may have been the result of the onset of optical saturation of the resonant transition. A nearly five order-of-magnitude increase in ionization signal was obtained by increasing the laser power by less than two and one-half orders of magnitude.

Thallium. The thallium transition at 291.8 nm differs from the thallium transition at 377.6 nm in several respects. Although the former does not originate at the ground state but at a low-lying thermally-populated level (see Table I), it is a somewhat stronger transition as indicated by its transition probability (Table I). The energy defect for this transition is $7,215 \text{ cm}^{-1}$, much smaller and more optimum for LEI work than that of the previous thallium transition. The energy overshoot for two-photon ionization using this transition is $27,041 \text{ cm}^{-1}$, and is the largest overshoot encountered in the present study. The log-log plot of LEI signal vs. laser power for this transition is shown in Figure 5. The ionization signal increases linearly with laser power until optical saturation occurs. Beyond the point of saturation, the signal continues to increase with a slope of about 0.5. This is in contrast with two-photon behavior observed for other elements for which the resonant transitions were optically saturated, resulting in slopes of one above the saturation plateau. Considering the small energy defect, and large two-photon energy overshoot associated with this resonant transition, it is likely that collisional ionization from the laser-populated level at $42,049 \text{ cm}^{-1}$ predominated over two-photon ionization even at the higher laser powers. The slope of 0.5 above the onset of saturation is puzzling, but may be a function of the relative contributions of the

two competing ionization mechanisms. In the complete absence of two-photon ionization, a slope of near zero would be expected beyond the onset of saturation.

CONCLUSION

The preceding experimental results illustrate that, for a variety of atomic transitions, both laser-induced collisional ionization (i.e., LEI) and resonant two-photon ionization occur in flames as a result of excitation of analyte atoms by a single laser source. The resonant two-photon ionization mechanism, where applicable, provides additional ionization yield in flames, beyond that which is possible with optically-saturated, single-step LEI using the same resonant transition. Several examples have been presented that illustrate the interaction between the competing mechanisms of LEI and resonant two-photon ionization in flames. Using these examples it should be possible to qualitatively predict the relative importance of collisional and direct photoionization processes. Table II summarizes the experimental data and indicates the optical saturation status of the resonant transition and whether or not second order laser power dependence was observed. In each case, the observed dependence of the ionization signal on incident laser power provided a means by which the ionization mechanism(s) could be characterized. The relative probabilities of the two mechanisms determine where along the ordinate of laser power they will occur. For example, when the energy defect between a laser-populated level and the ionization continuum was small, laser-induced collisional ionization was favored at low laser power, and two-photon ionization was apparent only at higher laser powers. However, when energetics dictated a low probability for collisional ionization (large energy defect), and conditions for two-photon ionization were favorable (small energy overshoot), the

latter contributed to the total signal even at low laser power. Resonant two-photon ionization in flames appears to be most effective where laser-induced collisional ionization is inefficient. Therefore, it is likely that the results of similar experiments carried out in the higher temperature air-acetylene flame would reflect the greater efficiency of collisional ionization in that flame.

The dependence of ionization yield on laser power observed in the present study differs from that of similar studies conducted for resonance ionization mass spectrometry. The absence of abundant collisional processes providing a competing ionization mechanism in RIS and RIMS allows the two-photon pathway to predominate throughout the range of irradiance. We have shown that for resonant two-photon ionization in flames, the characteristic second-order power dependence is not apparent when the resonant transition through which that mechanism proceeds is optically saturated. Optical saturation of the resonant transition used in RIS or RIMS also precludes observation of a second-order power dependence for the two-photon ionization process (2). However, the apparent laser power dependence of RIS or RIMS is more directly determined by illumination and detection geometries, and the true order of the quantum processes is often masked in those techniques as it is in the present work. It is highly probable that resonance ionization in flames suffers losses in spectral selectivity similar to those observed in RIS and RIMS due to saturation broadening of the resonant transition. This is not as serious a problem in RIMS because of the elemental selectivity afforded by the mass spectrometer (2). In addition, non-specific multiphoton ionization of sample matrix elements and native species in flames may also degrade spectral selectivity, thus, limiting the analytical utility of this approach.

ACKNOWLEDGMENT

Michael D. Seltzer was supported by an Office of Naval Technology Postdoctoral Fellowship which was administered by the American Society for Engineering Education.

LITERATURE CITED

1. C. J. Hurst, M.G. Payne, S.D. Kramer, and J.P. Young
Rev. Mod. Phys. **51**, 767 (1979)
2. J.D. Fassett, J.C. Travis, L.J. Moore, and F.E. Lytle
Anal. Chem. **55**, 765 (1983)
3. C.A. van Dijk, F.M. Curran, K.C. Lin, and S.R. Crouch
Anal. Chem. **53**, 1275 (1981)
4. M.D. Seltzer and R.B. Green
Appl. Spectrosc., Submitted for publication (1988)
5. J.C. Travis, G.C. Turk, and R.B. Green
Anal. Chem. **54**, 1007A (1982)
6. O. Axner, I. Lindgren, I. Magnusson, and H. Rubensztein-Dunlop
Anal. Chem. **57**, 776 (1985)
7. F.M. Curran, K.C. Lin, G.E. Leroi, P.M. Hunt, and S.R. Crouch
Anal. Chem. **55**, 2382 (1983)
8. P. Esherick,
Phys. Rev. A. **15**, 1920 (1977)

9. L.P. Hart, B.W. Smith, and N. Omenetto
Spectrochim. Acta. **40B**, 1637 (1985)

10. E.H. Piepmeier
Spectrochim. Acta **27B**, 431 (1972)

11. S. Speiser and S. Kimel
Chem. Phys. Lett. **7**, 19 (1970)

12. E.H. Piepmeier and G.J. Beenen
Appl. Spec. **36**, 235 (1982)

13. C.H. Corliss and W.R. Bozman "Experimental Transition Probabilities for
Spectral Lines of Seventy Elements", National Bureau of Standards Monograph
53 Washington, D.C. 1962

Table I

Relevant Energetics for Resonant Two-Photon Ionization

Element	λ Exc. (nm)	Energy Levels (cm^{-1})	Transition Probability* ($10^8/\text{sec}$)	Ionization Limit (cm^{-1})	Energy Defect (cm^{-1})	Energy Overshoot (cm^{-1})
Sr	293.2	0-34098	0.055	45926	11828	22270
Na	568.3	16973-34549	0.88	41450	6901	10675
Ga	294.4	826-34787	11	48380	13593	20368
Tl	377.6	0-26478	1.0	49264	22786	3692
Co	292.9	0-34134	0.043	63438	29304	4830
Tl	291.8	7793-42049	15	49264	7215	27041

*Ref. 13

Table II

Summary of Experimental Results

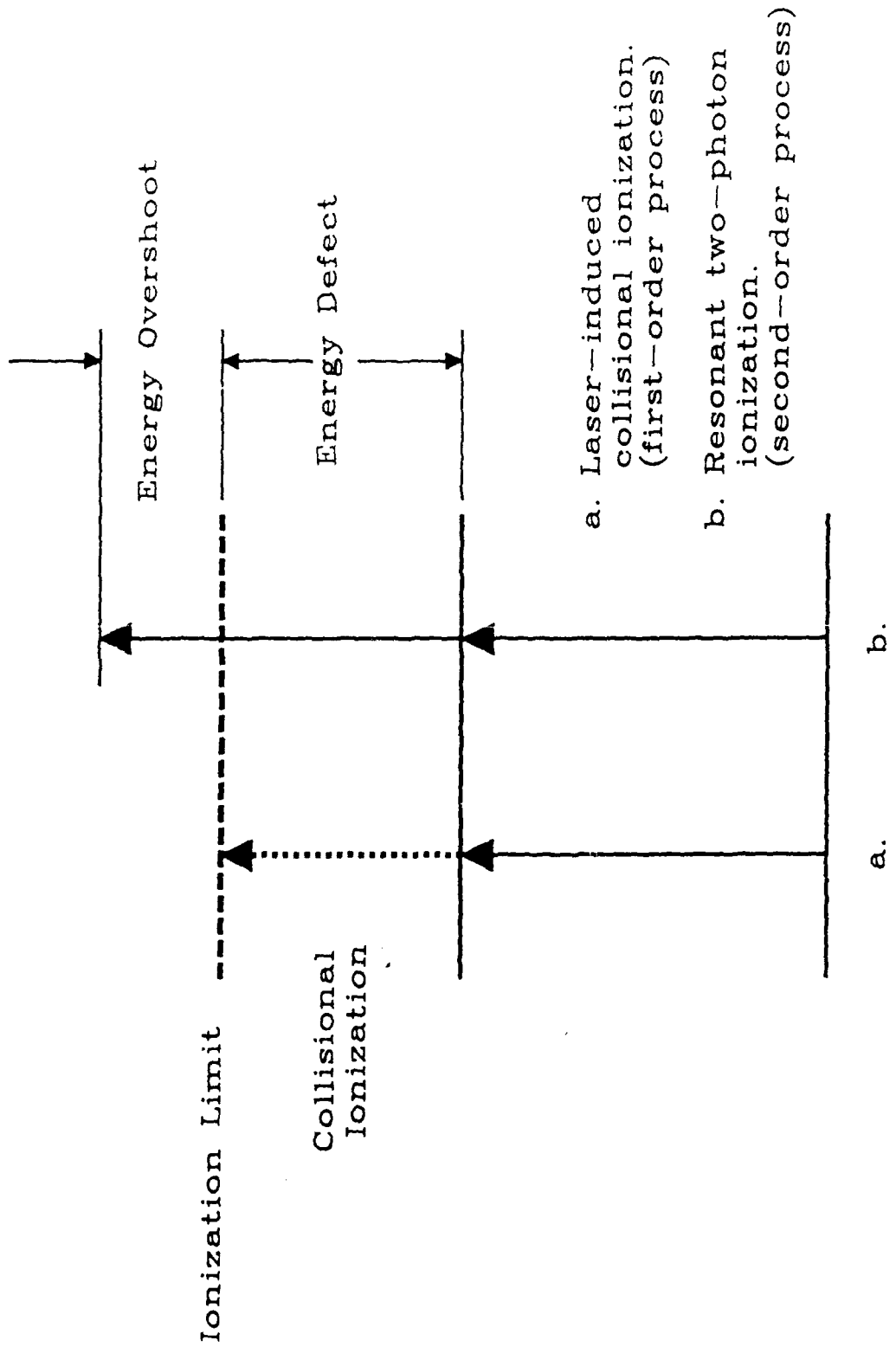
Element	Resonant Transition	Optical Saturation	Energy Defect	Energy Overshoot	Power Dependence*
Sr	293.2 nm	no	moderate	large	2nd order
Na	568.3 nm	yes	small	moderate	1st order
Ga	294.4 nm	yes	moderate	large	1st order
Tl	377.6 nm	yes	large	small	1st order
Co	292.9 nm	no	large	small	2nd order
Tl	291.8 nm	yes	small	large	1st order**

*Slope of log-log plot

**Slope < 1

FIGURE CAPTIONS

- Figure 1. Energy diagram illustrating the competing mechanisms of laser-induced collisional ionization and resonant two-photon ionization. Photons for resonant and photoionization step are of equal energy.
- Figure 2. Energy diagram and log-log plot of strontium ionization signal vs. laser power at 293.2 nm.
- Figure 3. Energy diagram and log-log plot of sodium ionization signal vs. laser power at 568.3 nm.
- Figure 4. Energy diagram and log-log plot of gallium ionization signal vs. laser power at 294.4 nm.
- Figure 5. Energy diagram and log-log plot of thallium ionization signal vs. laser power at 377.6 nm.
- Figure 6. Energy diagram and log-log plot of cobalt ionization signal vs. laser power at 292.9 nm.
- Figure 7. Energy diagram and log-log plot of thallium ionization signal vs. laser power at 291.8 nm.

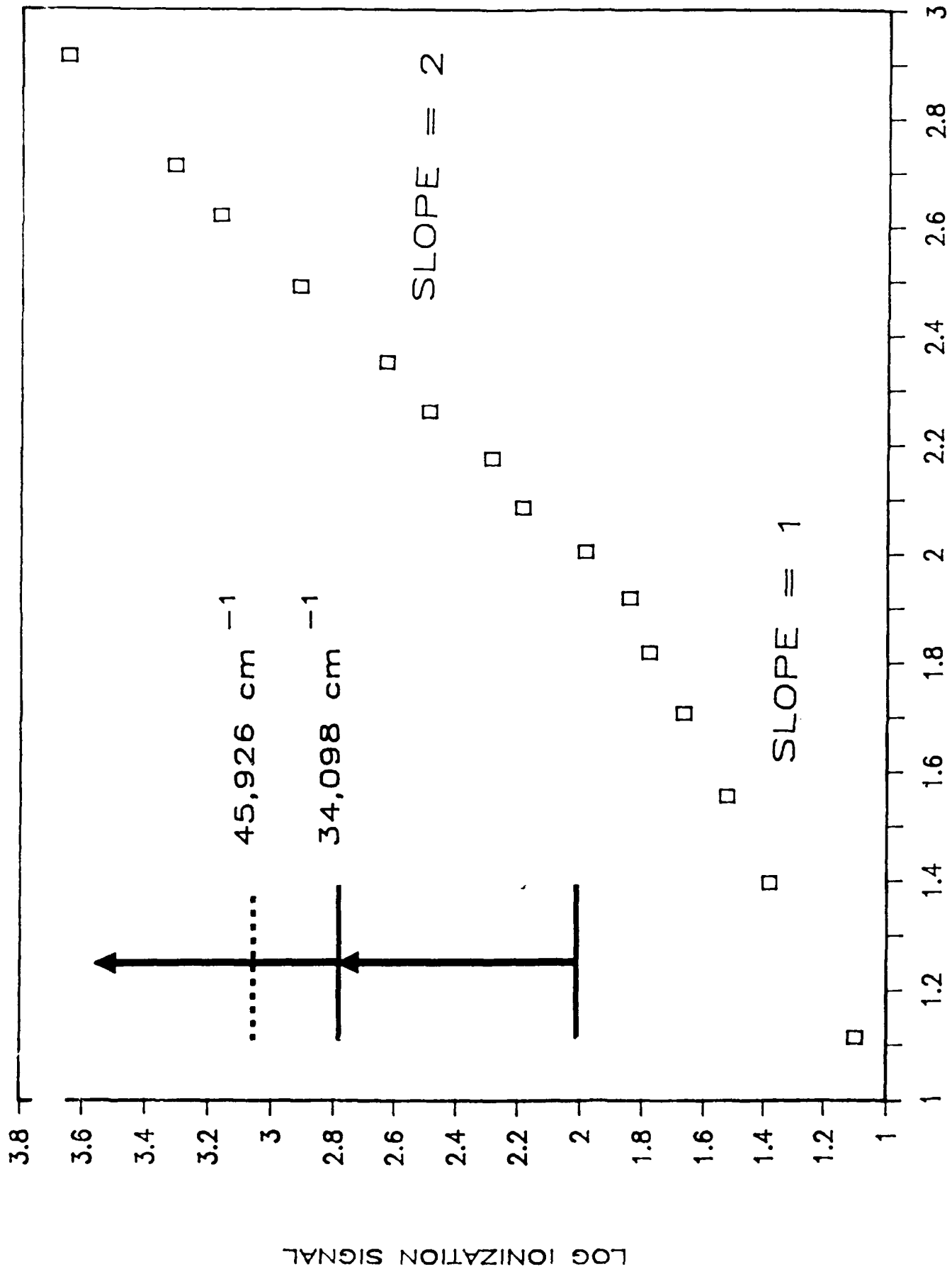


a. Laser-induced collisional ionization. (first-order process)

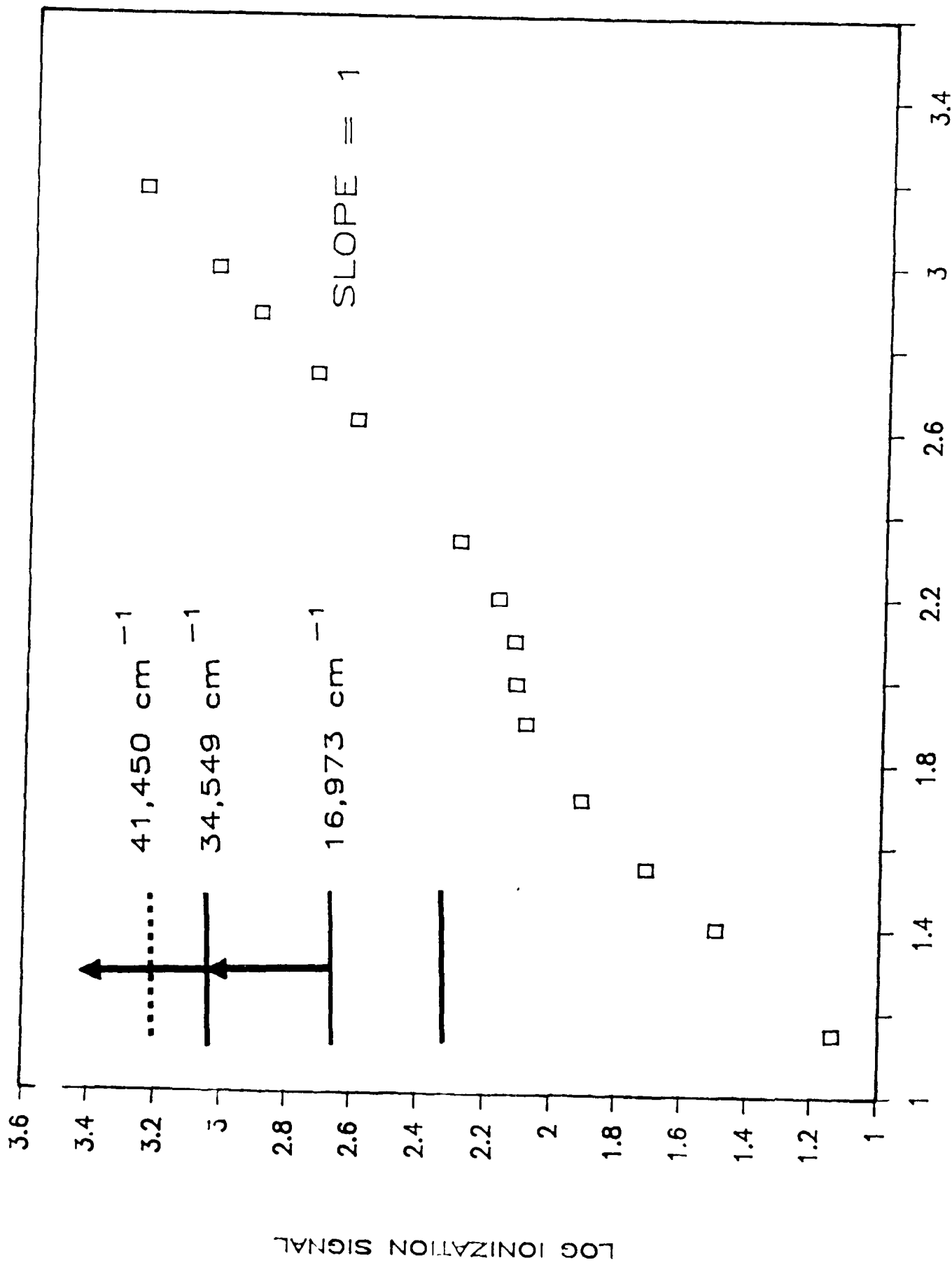
b. Resonant two-photon ionization. (second-order process)

b.

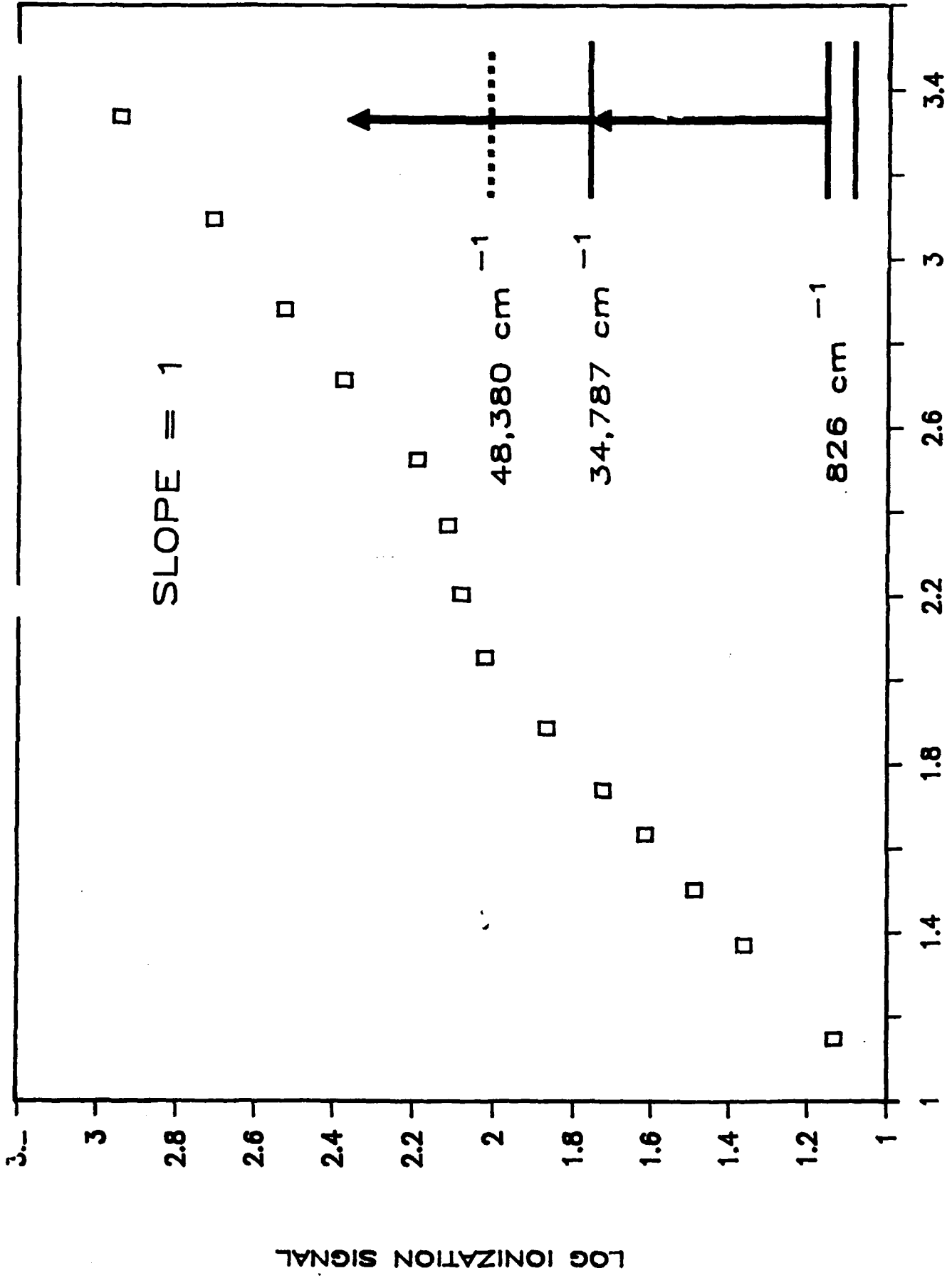
a.



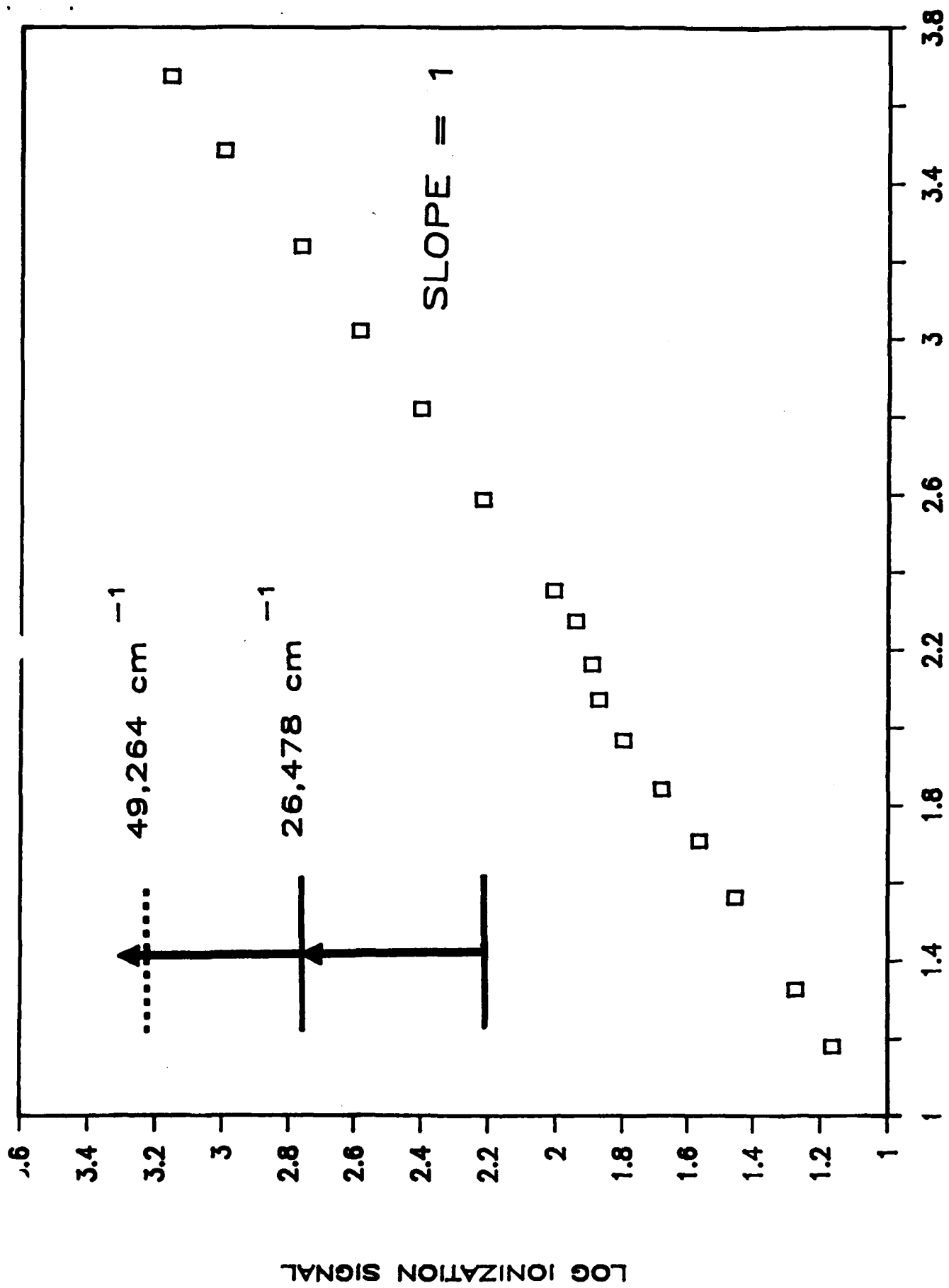
LOG LASER POWER AT 293.2 nm

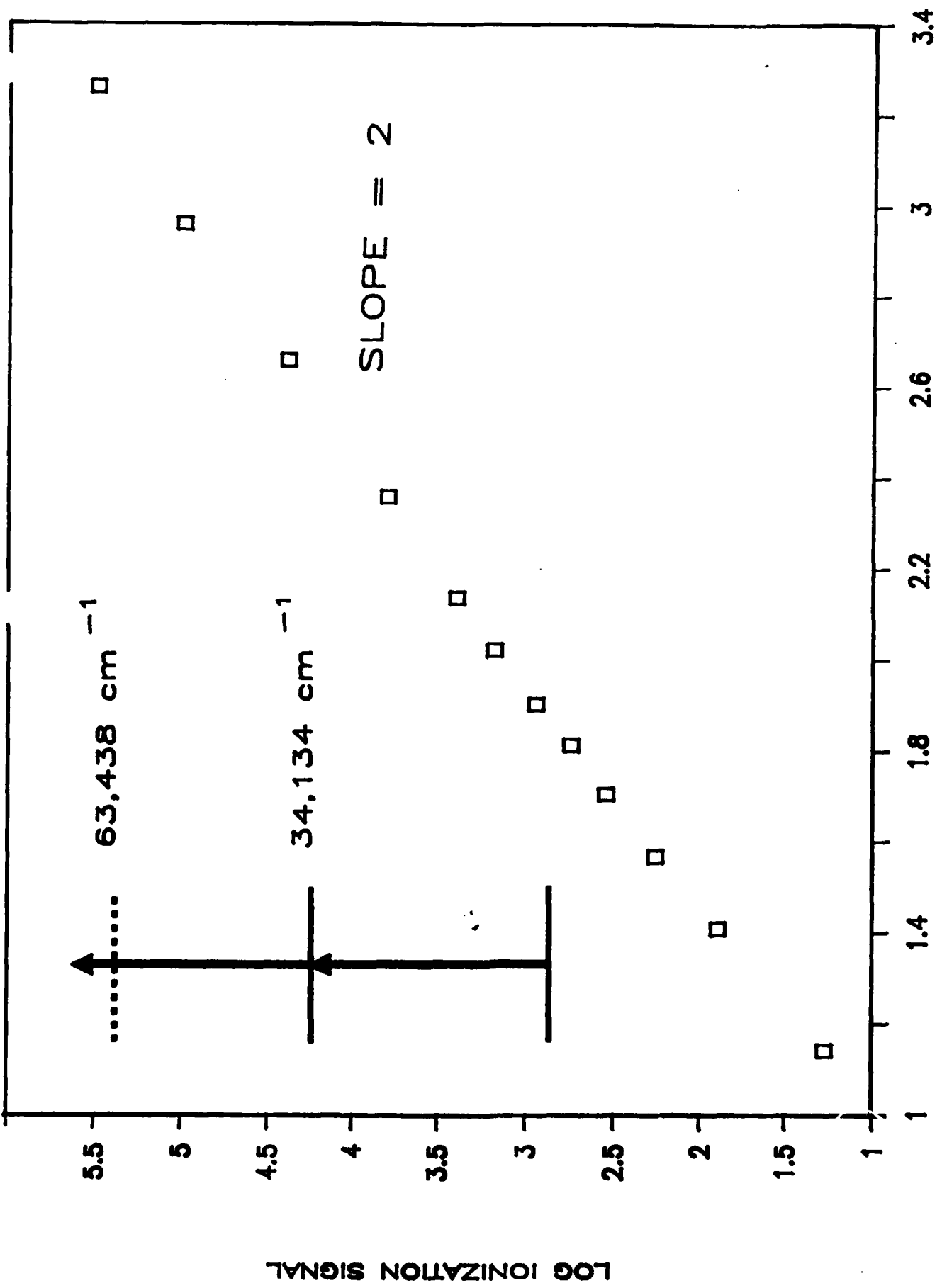


LOG LASER POWER AT 568.3 nm

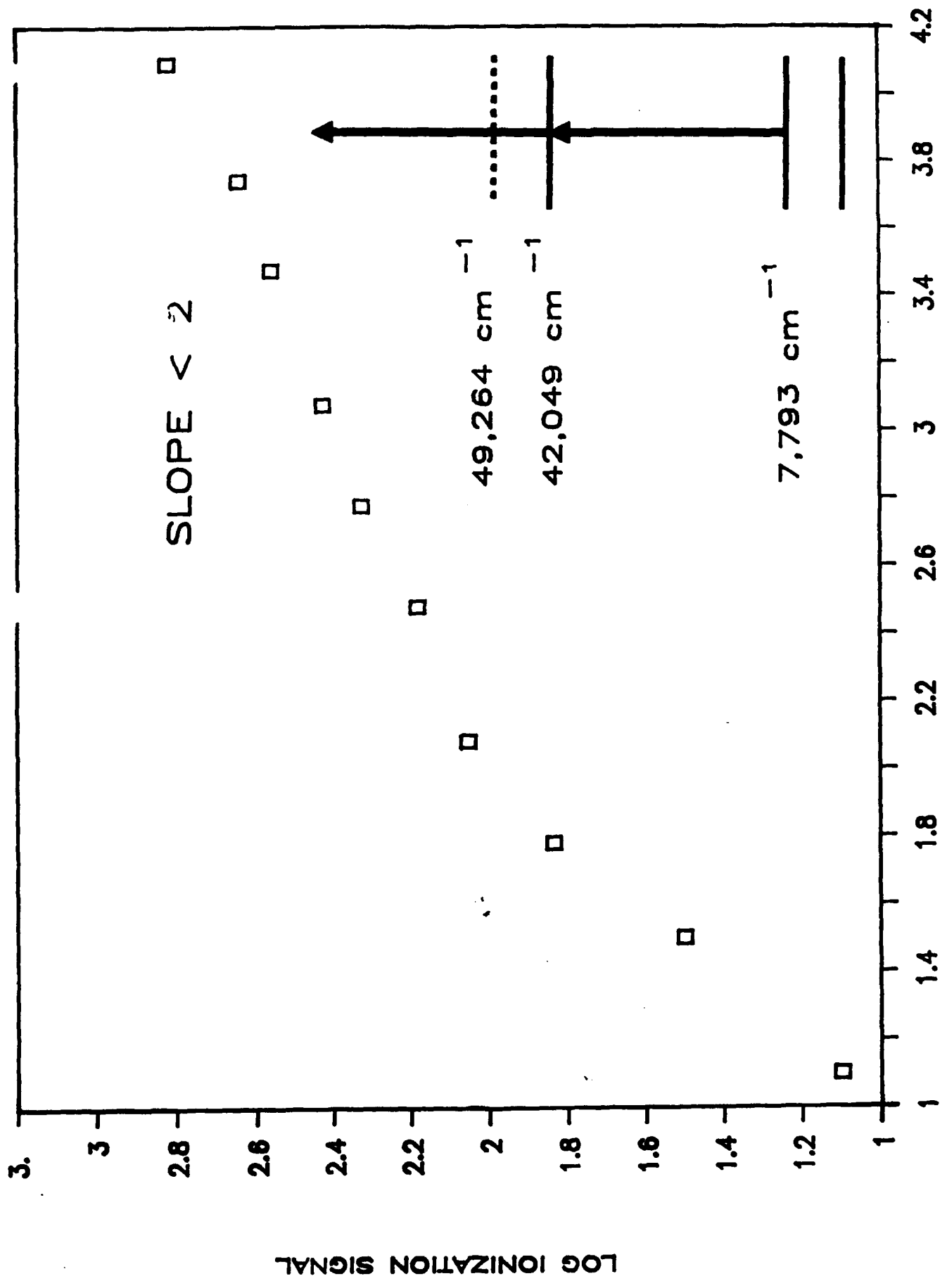


LOG LASER POWER AT 294.4 nm





LOG LASER POWER AT 292.9 nm



LOG LASER POWER AT 291.8 nm

ELECTRICAL CHARACTERISTICS OF MICROWAVE-INDUCED PLASMAS FOR LASER-INDUCED IONIZATION SPECTROMETRY

Key Words: Laser-induced Ionization, Microwave-induced Plasmas,
Active Nitrogen

M.D. Seltzer and R.B. Green

Research Department, Chemistry Division (Code 3851)
Naval Weapons Center, China Lake, CA 93555

ABSTRACT

The electrical properties of microwave-induced plasmas (MIPs), relevant to signal detection of laser-induced ionization, have been investigated. DC current vs. applied voltage relationships have been characterized for both argon and argon-active nitrogen plasmas. Suppression of signal detection for laser-induced ionization in the active nitrogen plasma is similar to that encountered in flames in the presence of thermally-ionized Group IA elements.

INTRODUCTION

This paper reports further developments in a previously reported investigation of the feasibility of laser-induced ionization in microwave-induced plasmas (MIPs) (1). In the previous study, an active nitrogen plasma was investigated as an atom reservoir for laser-enhanced ionization (LEI) and direct laser ionization (DLI). The active nitrogen was generated at atmospheric pressure by exciting a mixture of argon and nitrogen using a resonant microwave cavity. The plasma atom reservoir performed adequately to allow low picogram sensitivity for the test element indium which was introduced in discrete quantities using a microarc atomizer (2). We have also recently reported a detailed study of the background spectra obtained by laser-induced ionization of nitrogen in the plasma (3).

A goal of the previous investigation was to elucidate the role of the active nitrogen in the excitation and ionization process. One approach to this problem was to vary the concentration of active nitrogen in the plasma plume and observe the effect on the laser-induced ionization signal. It was anticipated that the efficacy of collisional ionization would be related to the active nitrogen concentration and that some optimum would be observed as nitrogen was added to the argon stream. To the contrary, it was observed that the LEI signal decreased as the percent nitrogen in the argon stream was increased and more active nitrogen was produced. The maximum signals were observed for minimum nitrogen flow rates into the plasma and low applied microwave power, both of which result in minimum production of the metastable nitrogen

species. However, ionization signals measured in a pure argon discharge were one to two orders of magnitude smaller than those with nitrogen added. We originally postulated that highly efficient excitation by increasing amounts of active nitrogen in the plasma may have resulted in partial depletion of ground state atoms, hence, the drop in sensitivity (1). It has been suggested that electrical suppression of ion detection by the highly-charged active nitrogen plasma may be responsible for the observed behavior (4). The purpose of the present study was to investigate some of the electrical characteristics of the microwave-induced plasma and evaluate their effect on ion detection.

EXPERIMENTAL SECTION

The instrumentation used in the present study is similar to that used in Ref. 1 with two exceptions. A 10 Hz Nd:YAG laser-pumped dye laser (Quantel, Santa Clara, CA) was used in the present study in place of the 30 Hz flashlamp-pumped dye laser. Also, a graphite furnace atomizer was modified to allow sample introduction into the MIP. Atomizer platforms made in the laboratory were inserted into the furnace tubes to delay sample atomization until the temperature of the entire tube was stabilized. Vaporized samples were entrained directly in the plasma gas flow (nitrogen and/or argon). Typical sample introduction reproducibility was 10% R.S.D.. Signal processing was facilitated by computerized data acquisition. The plasma plume was illuminated along its longitudinal axis with detection electrodes positioned symmetrically on either side of the plasma plume (1). A 0.22 m monochromator (Spex, Edison, NJ) and photomultiplier were used for fluorescence detection in a diagnostic experiment (see Results and Discussion).

RESULTS AND DISCUSSION

The concentration of active nitrogen in the plasma can be adjusted by varying the flow of nitrogen relative to the argon flow rate. In the previous study, it was not clear whether varying the plasma gas composition affected the plasma, the microarc atomizer, ion collection, or all three. Since the microarc employs a combination of sputtering and thermal desorption to atomize samples, it is probable that its performance is sensitive to gas composition. The graphite furnace atomizer used in the present study appeared to be unaffected by variations in the nitrogen/argon ratio and therefore should allow clarification of the effects of plasma gas composition on ionization signals relative to microarc sample introduction. Figure 1 illustrates the effects of varying the nitrogen flow rate into the plasma on the size of the LEI signals obtained for individual furnace atomizations of 1 ng samples of manganese, excited at 279.5 nm. Since the flow of nitrogen amounted to only a few percent of the total gas flow, sample transport was assumed to be reasonably constant. The applied

voltage for ion detection was -1000 V. Similarly to the previous study, the LEI signal was observed to decrease with increasing nitrogen flow rate and subsequent increases in the concentration of active nitrogen. However, the most significant difference in Figure 1 and previous results (1) is that the ionization signal in the present work was maximized when the nitrogen flow was reduced to zero resulting in a pure argon plasma. This suggests that in the previous study the microarc atomizer simply may have worked better when a small amount of nitrogen was present than in a pure argon atmosphere. The microarc cathode appeared to glow more brightly in the presence of nitrogen indicating higher temperatures which should facilitate thermal desorption of the sample. Since the effect of increasing nitrogen flow rates on ionization signals using graphite furnace atomization was otherwise similar to that for microarc atomization, atomization processes can be eliminated as the cause of the observed behavior.

Quenching of excited-state analyte atoms by ground state nitrogen molecules also presents a possible explanation for decreased ionization signals at high nitrogen flow rates. To evaluate this possibility, laser-excited atomic fluorescence was carried out using lead as a test element because of the availability of a direct-line excitation scheme. The lead resonance transition at 283.3 nm was excited and fluorescence was detected orthogonally at 405.8 nm. Fluorescence was detected for lead samples introduced into a pure argon discharge and discharges with increasing nitrogen flows. Differences in the fluorescence signal of approximately 10% were observed throughout suggesting that quenching effects due to increased nitrogen flow rates were negligible.

In analytically-useful flames where Group IA elements are thermally ionized to a large extent, suppression of analyte signal detection is a well-characterized problem (5). Signal suppression is due to the accelerated formation of a space charge in the region between the anode and cathode which forces the retraction of the detecting field to the immediate vicinity of the cathode. Analytically-useful flames such as the air-acetylene flame are usually characterized by high electrical resistance. In the presence of easily-ionized elements like sodium or potassium, the resistance of the flame is lowered substantially resulting in an increase in DC current through the flame when a voltage is applied across the flame. Figure 2 illustrates the effect of increasing the applied voltage across an air-acetylene flame on the DC current measured by connecting a digital multimeter in the electrode circuit. An electrode configuration similar to that used for signal detection in the active nitrogen plasma was used, i.e., plate electrodes were positioned symmetrically about the slot burner-supported flame. The lower trace in Figure 2 represents the behavior for an air-acetylene flame into which pure water has been aspirated. The data for the upper trace was obtained by aspirating a solution of 100 µg/mL sodium into the flame. The slopes are inversely proportional to the flame resistance. As can be seen in Figure

2, the DC current increases more rapidly with applied voltage when sodium is present in the flame at levels sufficient to produce space charge and subsequent suppression of the analyte ionization signal (5).

Figure 3 shows the results of a similar experiment performed in the microwave-induced argon and argon/active nitrogen plasmas. The applied voltage was varied and the resulting DC current was monitored. The DC current in the active nitrogen plasma increased rapidly with applied voltage compared to that in the pure argon discharge. Electrical arcing across the pure argon plasma limited the usable applied voltage. Arcing in the active nitrogen discharge did not occur until much higher applied voltages. Figures 2 and 3 are similar in form. Although the DC currents measured for the active nitrogen plasma are much lower than those observed for the sodium-seeded flame, they are greater than those measured for the pure argon discharge. This indicates that the resistance of the active nitrogen plasma is much lower making the formation of space charge in the active nitrogen more likely.

It is difficult to make a direct comparison between the active nitrogen plasma and the pure argon discharge for several reasons. The active nitrogen plasma includes long-lived metastable species which permit the plasma plume to propagate several centimeters downstream from the original point of discharge in the Beenakker cavity. The argon plasma dwells primarily inside the cavity although argon plasma species exist in the cavity outflow. (Otherwise the argon plasma would be useless in the present application.) Therefore, the active nitrogen plasma is more dense than the argon plasma at the point of signal detection (i.e., the region between the electrodes). This may account for the higher DC current observed in the active nitrogen plasma.

Since the active nitrogen plasma appears to be space-charge limited with respect to detection of laser-induced ionization and larger ionization signals are detected in the pure argon discharge, it is worth investigating the argon plasma as an alternative to the active nitrogen discharge. Preliminary results in this laboratory, using graphite furnace sample introduction into an argon MIP for LEI, indicate low picogram sensitivity for a few elements.

CONCLUSION

Further investigation of a microwave-induced atmospheric pressure active nitrogen plasma suggests that the highly ionized discharge is space-charge limited with respect to detection of laser-induced ionization. Preliminary indications are that a pure argon discharge, although lacking the robust excitation properties of the active nitrogen plasma, is less subject to space charge and may be more useful as an atom reservoir for laser-induced ionization spectrometry.

ACKNOWLEDGMENT

Michael D. Seltzer was supported by an Office of Naval Technology postdoctoral fellowship which was administered by the American Society for Engineering Education.

REFERENCES

1. M.D. Seltzer and R.B. Green, *Spectrosc. Lett.*, **20** (1987) 501
2. J.P. Harrison, R.D. Deutsch, and G.M. Hieftje, *Appl. Spectrosc.*, **37** (1983) 101
3. M.D. Seltzer, E.H. Piepmeyer, and R.B. Green, *Appl. Spectrosc.*, **42** (1988)
4. G.C. Turi, private communication.
5. R.B. Green, G.J. Havnilla, and T.O. Trask, *Appl. Spectrosc.*, **34** (1980) 561

FIGURE CAPTIONS

- Fig. 1. Effect of varying the nitrogen flow rate on the peak LEI signal for 1 ng samples of Mn. (The signal traces have been offset for clarity)
- Fig. 2. DC current vs. applied voltage for air-acetylene flame, with aspiration of deionized water and 100 $\mu\text{g/mL}$ Na solution.
- Fig. 3. DC current vs. applied voltage for microwave-induced argon and active nitrogen plasmas.

